

Emergence of tricritical point and liquid-gas phase in the massless $2 + 1$ dimensional Gross-Neveu model

Jean-Loïc Kneur,^{1,*} Marcus Benghi Pinto,^{2,†} Rudnei O. Ramos,^{3,‡} and Ederson Staudt^{2,§}

¹*Laboratoire de Physique Théorique et Astroparticules-CNRS-UMR 5207, Université Montpellier II, France*

²*Departamento de Física, Universidade Federal de Santa Catarina, 88040-900 Florianópolis, Santa Catarina, Brazil*

³*Departamento de Física Teórica, Universidade do Estado do Rio de Janeiro, 20550-013 Rio de Janeiro, Rio de Janeiro, Brazil*

(Received 24 May 2007; published 31 August 2007)

A complete thermodynamical analysis of the $2 + 1$ dimensional massless Gross-Neveu model is performed using the optimized perturbation theory. This is a nonperturbative method that allows us to go beyond the known large- N results already at lowest order. Our results, for a finite number of fermion species, N , show the existence of a tricritical point in the temperature and chemical potential phase diagram for a discrete chiral phase transition allowing us precisely to locate it. By studying the phase diagram in the pressure and inverse density plane, we also show the existence of a liquid-gas phase, which, so far, was unknown to exist in this model. Finally, we also derive N dependent analytical expressions for the order parameter, critical temperature, and critical chemical potential.

DOI: [10.1103/PhysRevD.76.045020](https://doi.org/10.1103/PhysRevD.76.045020)

PACS numbers: 11.10.Wx, 12.38.Cy, 11.15.Tk

I. INTRODUCTION

The Gross-Neveu (GN) model [1] has been extensively used as a prototype for quantum chromodynamics (QCD) and related issues. This is due to the fact that both models share some common features such as asymptotic freedom and chiral symmetry breaking (CSB). For this reason the GN model is useful as a toy model to test different techniques that can be ultimately used to tackle problems related to QCD phase transitions. At the same time, in the condensed matter physics domain, the two ($1 + 1$) dimensional GN model (GN2d) has been associated to polymers [2] including unidimensional molecules such as polyacetylene [3], while the three ($2 + 1$) dimensional version (GN3d) has been related to planar superconductors [4]. The applications concerning phase transitions within the GN model are commonly carried out in the finite temperature and/or finite density domain where nonperturbative techniques must be employed. In these applications the most commonly used analytical nonperturbative technique is the $1/N$ expansion [5] where, for the GN model, N represents the number of fermionic species (see Ref. [6] for a recent review). In general, this expansion is considered only at the leading order in what is known as the large- N approximation.

In the large- N approximation there are fundamental differences between the GN2d and GN3d models that are worth recalling. In dimensions $d = 2$ one observes chiral symmetry restoration (CSR) occurring via a phase transition of the second kind for high temperature (T) and small chemical potential (μ) values, while for low T and high μ the transition is of the first kind [7]. One finds a tricritical

point in the $T - \mu$ plane separating the second order transition line from the first order one, while metastable lines accompany the first order transition [7,8]. In the $P - 1/\rho$ plane (P being the pressure and ρ the density) one finds a phase diagram similar to the one generated by a Van der Waals liquid so that the CSB region corresponds to the “gas” phase while the CSR region corresponds to the “liquid” phase. It then follows that the first order transition allows for the appearance of a (mixed) liquid-gas phase. The chiral (dynamical) symmetry breaking happening in the massless GN2d with discrete symmetry at finite temperature, however, must be seen with care, since it is an artifact of the large- N approximation. This is a consequence of well-known no-go theorems concerning that there should be no discrete symmetry breaking in one space dimension [9]. In this case the system’s vacuum manifold allows for the appearance of kink-antikink configurations that are unsuppressed at any finite temperature [10]. The system becomes segmented into regions of alternating signs of the order parameter whose net average value becomes zero. At leading order, the $1/N$ approximation misses this effect because the energy per kink goes to infinity as $N \rightarrow \infty$, while the contribution from the kinks has the form e^{-N} . The large- N results for the GN model in $2 + 1$ dimensions are rather different [4]. First of all, as far a discrete chiral symmetry is concerned, the no-go theorem of one space dimension no longer applies (though now, in two space dimensions, the no-go theorem applies to the nonexistence of a continuous broken symmetry at any finite temperature). The GN3d phase diagram produced by the large- N approximation shows that the CSB/CSR transition is of the second kind everywhere except at $T = 0$, where it happens to be of the first kind. Within this approximation, there are no tricritical points lying in the $T - \mu$ plane and no liquid-gas phase. The model behaves more like a planar superconductor with the transition CSB/CSR happening as a superconducting/normal one [4].

*kneur@lpta.univ-montp2.fr

†marcus@fsc.ufsc.br

‡rudnei@uerj.br

§ederson@fsc.ufsc.br

Later, Kogut and Strouthos used lattice Monte Carlo simulations to study the GN3d at finite N [11]. They predicted that a tricritical point should exist at low finite values of T , but within the numerical precision of their simulations, they were unable to give its exact location (in earlier lattice simulations [12] used to obtain the phase diagram for the GN3d at finite N , some evidence for a tricritical point was also pointed out). No other attempts or approximations were able to improve on this situation. As far we are aware, no evidence has been given so far for a possible chiral “liquid-gas” kind of phase.

In an attempt to go beyond the simple large- N approximation and in such a way that temperature and chemical potential effects could be considered in a simple approximation method, three of the present authors [13] have recently considered the GN2d in the linear δ expansion method (LDE), also known as the optimized perturbation method (OPT). That study allowed for the inclusion of the first nontrivial finite N corrections to the complete phase diagram of the GN2d model. The main results of Ref. [13] are the derivation of analytic nonperturbative expressions, containing finite N corrections, scalar field expectation value, critical temperature T_c (at $\mu = 0$), critical chemical potential μ_c (at $T = 0$), as well as for the tricritical point (at $T \neq 0$ and $\mu \neq 0$). In the phase diagram, the predicted CSB region is reduced for finite values of N . The OPT expression for T_c predicts values that are lower than the ones predicted by the large- N approximation which, in the light of the Coleman-Mermin-Wagner-Landau theorem [9], can be viewed as an indication of convergence.

Our recent success in treating the GN2d [13] and the previous lattice Monte Carlo results on the GN3d, concerning the eventual existence of a tricritical point in the GN3d model [11,12], gave us the motivation to investigate the GN3d using the OPT method to fully study its thermodynamics in order to confirm, in an analytical way, the existence of a tricritical point. The OPT method is known for exactly reproducing the large- N result for the effective potential (or free energy) already at the first nontrivial order [13,14]. The *perturbative* computation of higher orders brings finite N corrections, and nonperturbative results are generated upon using a variational criterion. One advantage is that at any perturbative order one has complete control over the contributions, while the eventual technical difficulties are like the ones one should encounter in a traditional perturbative computation. The convergence properties of the OPT in critical problems associated to Bose-Einstein condensates have been proved [15,16]. It is worth mentioning that some of the most accurate numerical results regarding the critical temperature for weakly interacting homogeneous Bose gases have also been obtained with this method [17]. Concerning the GN3d model the results obtained in the present work include analytical equations for both T_c (at $\mu = 0$) and μ_c (at $T = 0$) as well as for the scalar field vacuum expectation value (VEV) $\bar{\sigma}_c$

with finite N corrections. Contrary to the GN2d case, these values appear to be higher than the predicted large- N values. One of our most important results concerns the location of a tricritical point at finite values of T and μ . Being able to specialize to *any* value of N we choose $N = 3$, which is the relevant value for QCD. In a preliminary work [18], we already have shown that the unstable region in the $T - \mu$ plane, which corresponds to the region inside the metastable lines that accompany the first order transition line, is rather small, thus explaining the difficulty in observing and locating the tricritical point in previous works. Here we extend that work and, from the (Landau) free energy, or effective potential, we obtain other relevant thermodynamical quantities such as the thermodynamical potential, pressure, density, etc. This allows us to obtain the phase diagram in the intuitively more accessible $P - 1/\rho$ plane, and that shows how important the finite N corrections in the GN3d are. In fact, these corrections produce a phase diagram that is like a Van der Waals liquid, and *contrary* to the large- N predictions, we show that the model can display a mixed liquid-gas phase, which was previously unknown to exist.

This work is organized as follows. In the next section we present the GN model. In Sec. III we present the OPT method and the interpolated GN model, evaluating the effective potential in this nonperturbative scheme. We show that, already at leading order, our results go beyond the known large- N results. In Sec. IV we present the optimized results obtained from the effective potential at finite temperature and chemical potential. The dynamically generated fermion mass that we here associate with the auxiliary scalar field vacuum expectation value, the critical temperature, and critical chemical potential for chiral symmetry restoration are evaluated and explicit analytical expressions for these quantities are obtained. In this same section we also discuss the complete phase diagram for the GN model in the T and μ plane that then shows the presence of a tricritical point joining the lines of second order and first order chiral phase transitions, which we are able to locate precisely. In Sec. V we present other relevant thermodynamical quantities and show explicitly the existence of a mixed chiral symmetry restored/broken phase, the analogue of a liquid-gas phase in the $P - 1/\rho$ plane. The entropy, latent heat, and other important quantities are also evaluated. In Sec. VI we present the next order results, at $T = 0$ and $\mu = 0$, that allows us to assess the convergence of the OPT in this model. Our conclusions are presented in Sec. VII. Three appendices are included to show some technical details and the renormalization for the interpolated model up to second order.

II. THE GROSS-NEVEU MODEL

The Gross-Neveu model is described by the Lagrangian density for a fermion field ψ_k ($k = 1, \dots, N$) given by [1]

$$\mathcal{L} = \bar{\psi}_k(i\cancel{\partial})\psi_k + m_f\bar{\psi}_k\psi_k + \frac{g^2}{2}(\bar{\psi}_k\psi_k)^2, \quad (2.1)$$

where the summation over fermionic species is implicit in the above equation, with, e.g., $\bar{\psi}_k\psi_k = \sum_{k=1}^N \bar{\psi}_k\psi_k$. When $m_f = 0$, the theory is invariant under the discrete transformation¹

$$\psi \rightarrow \gamma_5\psi, \quad (2.2)$$

displaying a discrete chiral symmetry. For the studies of the model Eq. (2.1) in the large- N limit it is convenient to redefine the four-fermion interaction as $g^2N = \lambda$. Since g^2 vanishes like $1/N$ we study the theory in the large- N limit with fixed λ (see, e.g., [5]).

At finite temperature and density the model can be studied in terms of the grand partition function given by

$$Z(\beta, \mu) = \text{Tr} \exp[-\beta(H - \mu Q)], \quad (2.3)$$

where β is the inverse of the temperature, μ is the chemical potential, H is the Hamiltonian corresponding to Eq. (2.1), and $Q = \int dx \bar{\psi}_k \gamma_0 \psi_k$ is the conserved charge. Transforming Eq. (2.3) to the form of a path integral in the imaginary time (Euclidean) formalism of finite temperature field theory [19], we then have

$$Z(\beta, \mu) = \int \prod_{k=1}^N D\bar{\psi}_k D\psi_k \exp\{-S_E[\bar{\psi}_k, \psi_k]\}, \quad (2.4)$$

where the Euclidean action reads

$$S_E[\bar{\psi}_k, \psi_k] = \int_0^\beta d\tau \int dx \left[\bar{\psi}_k(\cancel{\partial} + \mu\gamma_0 - m_f)\psi_k - \frac{\lambda}{2N}(\bar{\psi}_k\psi_k)^2 \right], \quad (2.5)$$

and the functional integration in Eq. (2.4) is performed over the fermion fields satisfying the antiperiodic boundary condition in Euclidean time: $\psi_k(x, \tau) = -\psi_k(x, \tau + \beta)$.

III. THE EFFECTIVE POTENTIAL FOR THE INTERPOLATED THEORY

Let us now turn our attention to the implementation of the OPT method within the GN model. Usually, when employing this approximation one starts by performing a linear interpolation on the original model in terms of a fictitious parameter δ (used only for bookkeeping purposes), which allows for further expansions. According to this OPT interpolation prescription [20] (for a long, but far from complete list of references on the method, see [21]) the deformed four-fermion theory reads [13]

$$\mathcal{L}_\delta(\psi, \bar{\psi}) = \bar{\psi}_k(i\cancel{\partial})\psi_k + (1 - \delta)\eta\bar{\psi}_k\psi_k + \delta\frac{\lambda}{2N}(\bar{\psi}_k\psi_k)^2. \quad (3.1)$$

So, at $\delta = 0$ we have a theory of free fermions while at $\delta = 1$ the original theory is reproduced. Now, the introduction of an auxiliary scalar field σ can be achieved by adding the quadratic term,

$$-\frac{\delta N}{2\lambda}\left(\sigma + \frac{\lambda}{N}\bar{\psi}_k\psi_k\right)^2, \quad (3.2)$$

to $\mathcal{L}_\delta(\psi, \bar{\psi})$. We are then led to the interpolated model

$$\mathcal{L}_\delta = \bar{\psi}_k(i\cancel{\partial})\psi_k - \delta\sigma\bar{\psi}_k\psi_k - (1 - \delta)\eta\bar{\psi}_k\psi_k - \frac{\delta N}{2\lambda}\sigma^2 + \mathcal{L}_{ct,\delta}, \quad (3.3)$$

where $\mathcal{L}_{ct,\delta}$ is the part of Lagrangian density containing the necessary counterterms for renormalization, whose coefficients are allowed to be δ and η dependent [22,23]. As is well-known, the 2 + 1 dimensional GN model is not renormalizable in the usual perturbative expansion, but is renormalizable in the $1/N$ expansion [24], which has the property of modifying nonperturbatively the usual behavior under power counting. Though our renormalization procedure in the OPT expansion is more similar to a perturbative renormalization, this is not a real obstacle for our analysis. On general grounds it is always possible to calculate physical quantities in a nonrenormalizable model, at the price of introducing new counterterms at successive orders, which simply means that the sensitivity to an implicit cutoff of the model is expected to be more pronounced than in a renormalizable theory [25]. Such a procedure is commonly and successfully applied in many effective theories, like, e.g., typically in chiral perturbation theory (for a recent review of chiral perturbation theory with emphasis on the renormalization procedure see, e.g., [26] and references therein). However, concretely in our case, at first order of the OPT expansion all the relevant quantities are actually finite (when using dimensional regularization as we do here), thus completely unambiguous. Next, at second order, that we also investigate to some extent in this paper, it turns out that the only potentially nonrenormalizable contributions to the effective potential actually vanish, such that only standard (i.e., mass, wave function, etc.) counterterms are necessary to cancel the divergences. It should be mentioned, however, that this is somehow an accident of using dimensional regularization, which therefore delays at most, i.e., to much higher orders, the necessary introduction of new counterterms in our case. A detailed account for renormalization of the GN3d model in the OPT up to second order will be presented in Appendices B and C.

From the Lagrangian density in the interpolated form, Eq. (3.3), we can immediately read the corresponding new Feynman rules in Minkowski space. Each Yukawa vertex

¹Note that in $d = 3$ this is only true if one considers 4×4 Dirac matrices.

carries a factor $-i\delta$ while the (free) σ propagator is now $-i\lambda/(N\delta)$. The LDE dressed fermion propagator is

$$S_F(P) = \frac{i}{\not{P} - \eta_* + i\epsilon}, \quad (3.4)$$

where

$$\eta_* = \eta - (\eta - \sigma_c)\delta. \quad (3.5)$$

Any quantity computed from the above rules, at some finite order in δ , is dependent on the parameter η , which then must be fixed somehow. Here, as in most of the previous references on the OPT method, η is fixed by using the principle of minimal sensitivity (PMS). In the PMS procedure one requires that a physical quantity $\Phi^{(k)}$, that is calculated perturbatively to some k -th order in δ , be evaluated at the point where it is less sensitive to this parameter. This criterion then translates into the variational relation [27]

$$\left. \frac{d\Phi^{(k)}}{d\eta} \right|_{\bar{\eta}, \delta=1} = 0. \quad (3.6)$$

The optimum value $\bar{\eta}$ that satisfies Eq. (3.6) must be a function of the original parameters, including the couplings, thus generating nonperturbative results.

The OPT effective potential

The different contributions to the order δ^2 self-energy are displayed in Fig. 1. We can use these self-energy terms to evaluate the vacuum graphs contributing to the effective potential as shown in Fig. 2

In the following we make use of the following notations. The four-momentum P is given by $P = (P_0, \mathbf{p})$, where $P_0 = i(\omega_n - i\mu)$, with $\omega_n = (2n + 1)\pi T$, $n = 0, \pm 1, \pm 2, \dots$, are the Matsubara frequencies for fermions. The momentum integrals, when passing from Minkowski to Euclidean space-time, we here denote by

$$-i \int_p^{(T)} \equiv T \sum_{n=-\infty}^{+\infty} \int \frac{d^{d-1}p}{(2\pi)^{d-1}},$$

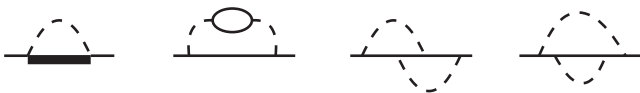


FIG. 1. Diagrams contributing to the self-energy to order δ^2 . The thick continuous fermionic lines represent η_* dependent terms which must be further expanded, while the thin continuous lines represent η dependent fermionic propagators and the dashed lines represent the σ propagator. Diagrams (a) and (b) (of order δ and order δ^2 , respectively) contribute with $1/N$, while diagrams (c) and (d) (both of order δ^2) contribute with $1/N^2$. Within dimensional regularization only graphs (b) and (c) are divergent. Tadpole graphs are not shown as they do not contribute to the effective potential nor to the counterterms (in $d = 2 + 1$) at the perturbative order we restrict ourselves to.

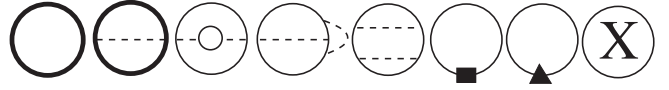


FIG. 2. Diagrams contributing to V_{eff}/N to order δ^2 . The thick continuous fermionic lines represent η_* dependent terms which must be further expanded while the thin continuous lines represent η dependent fermionic propagators and the dashed lines represent the σ propagator. The first (order δ^0) contributes with $1/N^0$, the second and third (order δ and order δ^2 respectively) contribute with $1/N$. The fourth and fifth (both of order δ^2) contribute with $1/N^2$. The sixth and seventh represent contributions due to the mass and wave function renormalization counterterms, respectively. The last graph represents the zero point energy subtraction term.

where all space momentum integrals are performed using dimensional regularization, $d = 3 - \epsilon$. The renormalization procedure (which is only necessary at order δ^2 since all relevant quantities are explicitly finite at order δ) is carried out in the modified minimal subtraction scheme ($\overline{\text{MS}}$).

The order δ OPT effective potential is obtained from the first two diagrams shown in Fig. 2 and, using the previous Feynman rules for the GN in the OPT, it is given by

$$\begin{aligned} \frac{V_{\text{eff}, \delta^1}(\sigma_c, \eta)}{N} &= \delta \frac{\sigma_c^2}{2\lambda} + i \int_p^{(T)} \text{tr} \ln(\not{P} - \eta) \\ &+ \delta i \int_p^{(T)} \text{tr} \frac{\eta - \sigma_c}{\not{P} - \eta + i\epsilon} + \frac{\Delta V_{\text{eff}}^{(a)}}{N}, \end{aligned} \quad (3.7)$$

where $\Delta V_{\text{eff}}^{(a)}/N$ brings the first $1/N$ correction to the effective potential shown by the second diagram in Fig. 2. This is given by [28]

$$\frac{\Delta V_{\text{eff}}^{(a)}}{N} = -\frac{i}{2N} \int_p^{(T)} \text{tr} \left[\frac{\Sigma_a(\eta)}{\not{P} - \eta + i\epsilon} \right], \quad (3.8)$$

where the trace is over Dirac's matrices only² while the term Σ_a represents the first contribution shown in Fig. 1 to the fermion self-energy,

$$\Sigma_a(\eta) = -\delta \frac{\lambda}{N} i \int_q^{(T)} \frac{1}{\not{Q} - \eta + i\epsilon}. \quad (3.9)$$

After taking the traces in Eq. (3.7) and rearranging the terms one obtains

²The factor -1 corresponding to a closed fermionic has already been taken into account [28].

$$\begin{aligned} \frac{V_{\text{eff},\delta^1(\sigma_c, \eta)}{N} &= \delta \frac{\sigma_c^2}{2\lambda} + 2i \int_p^{(T)} \ln(P^2 - \eta^2) \\ &+ 84i \int_p^{(T)} \frac{\eta(\eta - \sigma_c)}{P^2 - \eta^2 + i\epsilon} \\ &+ \delta \frac{2\lambda}{N} \eta^2 \left[i \int_p^{(T)} \frac{1}{P^2 - \eta^2 + i\epsilon} \right]^2 \\ &+ \delta \frac{2\lambda}{N} \left[i \int_p^{(T)} \frac{P_0}{P^2 - \eta^2 + i\epsilon} \right]^2. \end{aligned} \quad (3.10)$$

Then, at finite temperature and chemical potential, one finds (see Appendix A for the relevant integrals and Matsubara sums leading to this result)

$$\begin{aligned} \frac{V_{\text{eff},\delta^1(\sigma_c, \eta)}{N} &= \delta \frac{\sigma_c^2}{2\lambda} + \frac{|\eta|^3}{3\pi} + \frac{|\eta|T^2}{\pi} I_1(a, b) + \frac{T^3}{\pi} I_2(a, b) \\ &- \delta \frac{\eta(\eta - \sigma)}{\pi} [|\eta| + TI_3(a, b)] \\ &+ \delta \frac{\lambda\eta^2}{2(2\pi)^2 N} [|\eta| + TI_3(a, b)]^2 \\ &+ \delta \frac{\lambda T^4}{2(2\pi)^2 N} [I_4(a, b)]^2, \end{aligned} \quad (3.11)$$

where we have defined the functions

$$I_1(a, b) = \text{Li}_2[-e^{-(a-b)}] + \text{Li}_2[-e^{-(a+b)}], \quad (3.12)$$

$$I_2(a, b) = \text{Li}_3[-e^{-(a-b)}] + \text{Li}_3[-e^{-(a+b)}], \quad (3.13)$$

$$I_3(a, b) = \ln[1 + e^{-(a-b)}] + \ln[1 + e^{-(a+b)}], \quad (3.14)$$

$$\begin{aligned} I_4(a, b) &= \text{sgn}(\mu) \left[a \ln \left(\frac{1 + e^{a+b}}{1 + e^{a-b}} \right) + \text{Li}_2[-e^{a+b}] \right. \\ &\left. - \text{Li}_2[-e^{a-b}] \right], \end{aligned} \quad (3.15)$$

with $a = |\eta|/T$ and $b = |\mu|/T$.

The $T \rightarrow 0$ limit for each of the elements appearing in Eq. (3.11) are:

$$\lim_{T \rightarrow 0} T^2 I_1(a, b) = -\frac{1}{2} (|\mu| - |\eta|)^2 \theta(|\mu| - |\eta|), \quad (3.16)$$

$$\lim_{T \rightarrow 0} T^3 I_2(a, b) = \frac{1}{6} (|\eta| - |\mu|)^3 \theta(|\mu| - |\eta|), \quad (3.17)$$

$$\lim_{T \rightarrow 0} TI_3(a, b) = (|\mu| - |\eta|) \theta(|\mu| - |\eta|), \quad (3.18)$$

$$\lim_{T \rightarrow 0} T^2 I_4(a, b) = \frac{1}{2} \text{sgn}(\mu) (\eta^2 - \mu^2) \theta(|\mu| - |\eta|), \quad (3.19)$$

where $\theta(|\mu| - |\eta|)$ is the step function.

IV. OPTIMIZATION AND NUMERICAL RESULTS BEYOND LARGE- N

Before proceeding to the specific $d = 3$ case, considered in this work, let us apply the PMS to the most general order δ effective potential, which is given by Eq. (3.10). This exercise will help the reader to visualize the way the OPT-PMS resums the perturbative series. Setting $\delta = 1$ and applying the PMS to Eq. (3.10) we obtain that

$$\begin{aligned} &\left\{ \left[\eta - \sigma_c + \eta \frac{\lambda}{N} \left(i \int_p^{(T)} \frac{1}{P^2 - \eta^2 + i\epsilon} \right) \right] \left(1 + \eta \frac{d}{d\eta} \right) \right. \\ &\quad \times \left[i \int_p^{(T)} \frac{1}{P^2 - \eta^2 + i\epsilon} \right] + \frac{\lambda}{N} \left(i \int_p^{(T)} \frac{P_0}{P^2 - \eta^2 + i\epsilon} \right) \\ &\quad \left. \times \frac{d}{d\eta} \left(i \int_p^{(T)} \frac{P_0}{P^2 - \eta^2 + i\epsilon} \right) \right\} \Big|_{\eta=\bar{\eta}} = 0. \end{aligned} \quad (4.1)$$

As one can see in Appendix A, Eq. (A3), the last term of the above equation only survives when $\mu \neq 0$. In the case $\mu = 0$, Eq. (4.1) factorizes in a nice way which allows us to understand the way the OPT-PMS procedure resums the series producing nonperturbative results. With this aim one can easily check that (at $\delta = 1$)

$$\Sigma_a(\eta, T, \mu) = -\frac{\lambda}{N} \eta \left[i \int_p^{(T)} \frac{1}{P^2 - \eta^2 + i\epsilon} \right]. \quad (4.2)$$

Then, when $\mu = 0$, the PMS equation factorizes to

$$\begin{aligned} &[\bar{\eta} - \sigma_c - \Sigma_a(\bar{\eta}, T, \mu = 0)] \left(1 + \bar{\eta} \frac{d}{d\bar{\eta}} \right) \\ &\quad \times \left[i \int_p^{(T)} \frac{1}{P^2 - \bar{\eta}^2 + i\epsilon} \right] = 0, \end{aligned} \quad (4.3)$$

leading to the self-consistent relation

$$\bar{\eta} = \sigma_c + \Sigma_a(\bar{\eta}, T, \mu = 0), \quad (4.4)$$

which is valid for any temperature and number of space-time dimensions. In this way the OPT fermionic loops get contributions containing σ_c as well as rainbow (exchange) type of self-energy terms, like the first graph of Fig. 1. Note that when $N \rightarrow \infty$, $\bar{\eta} = \sigma_c$ and the large N result is exactly reproduced [13]. The mathematical possibility

$$i \int_p^{(T)} \frac{1}{P^2 - \bar{\eta}^2 + i\epsilon} = 0 \quad (4.5)$$

corresponds to the unphysical, coupling-independent solution discussed in Ref. [13]. Note that in the $d = 3$ case one obtains

$$\Sigma_a(\eta, T, \mu) = \frac{\lambda\eta}{4\pi N} [|\eta| + TI_3(a, b)]. \quad (4.6)$$

For numerical purposes, taking $\lambda \rightarrow -\lambda$ and defining $\Lambda = \pi/|\lambda|$, one can consider the dimensionless PMS equation:

$$\left\{ \left[\eta - \sigma_c + \frac{\eta}{4N} (|\eta| + TI_3(a, b)) \right] \left(1 + \eta \frac{d}{d\eta} \right) \right. \\ \left. \times (|\eta| + TI_3(a, b)) + \frac{T^4}{4N} I_4(a, b) \frac{d}{d\eta} I_4(a, b) \right\} \Big|_{\eta=\bar{\eta}} = 0, \quad (4.7)$$

where η , σ_c , T , and μ are in units of Λ .

A The $T = 0$ and $\mu = 0$ case

Let us start by analyzing each of the different possible cases involving the temperature and chemical potential corrections. For $T = 0$ and $\mu = 0$ we have that, to order δ ,

$$\frac{V_{\text{eff}}^{\delta^1}(\eta, \sigma_c)}{N} = \delta \frac{\sigma_c^2}{2\lambda} + \frac{|\eta|^3}{3\pi} - \delta \frac{\eta(\eta - \sigma_c)|\eta|}{\pi} \\ + \delta \frac{\lambda \eta^2 |\eta|^2}{2(2\pi)^2 N}. \quad (4.8)$$

Note that $V_{\text{eff}}^{\delta^1}(\eta, \sigma_c) = V_{\text{eff}}^{\delta^1}(-\eta, -\sigma_c)$, and by the virtue of this symmetry we shall look for $\bar{\eta}(\sigma_c)$ only for $\sigma_c > 0$, since for $\sigma_c < 0$ it is obvious that $\bar{\eta}(\sigma_c) = -\bar{\eta}(-\sigma_c)$.

Then, using $\lambda \rightarrow -\lambda$ and $\Lambda = \pi/|\lambda|$, one can write the free energy, at $T = 0$ and $\mu = 0$, as

$$\frac{V_{\text{eff}}^{\delta^1}(\eta, \sigma_c)}{N} = -\delta \frac{\sigma_c^2 \Lambda}{2\pi} + \frac{\eta^3}{3\pi} - \delta \frac{\eta^2(\eta - \sigma_c)}{\pi} - \delta \frac{\eta^4}{8\pi N \Lambda}, \quad (4.9)$$

where the notation is consistent with the fact that we are only interested in $\sigma_c > 0$ (in this case only $\eta > 0$ can recover the large- N result as $N \rightarrow \infty$ as can be seen from the PMS solution, Eq. (4.4)). Then $dV_{\text{eff}}/d\sigma_c = 0$ at $\sigma_c = \bar{\sigma}_c$ gives

$$\bar{\sigma}_c = \eta^2/\Lambda. \quad (4.10)$$

At the same time the PMS equation $dV_{\text{eff}}/d\eta = 0$ at $\eta = \bar{\eta}$ gives the relation

$$\bar{\eta} = \bar{\sigma}_c - \frac{\bar{\eta}^2}{4N\Lambda}, \quad (4.11)$$

from which we then obtain the expression

$$\bar{\eta} = \bar{\sigma}_c \mathcal{F}(N), \quad (4.12)$$

with the function $\mathcal{F}(N)$ defined as

$$\mathcal{F}(N) = 1 - \frac{1}{4N}. \quad (4.13)$$

The above results then lead to the *optimized* value for the (dynamically generated) vacuum expectation value for the scalar field, also shown in [18],

$$\bar{\sigma}_c = \frac{\Lambda}{\mathcal{F}(N)^2}. \quad (4.14)$$

This result is contrasted with the large- N result in Fig. 3.

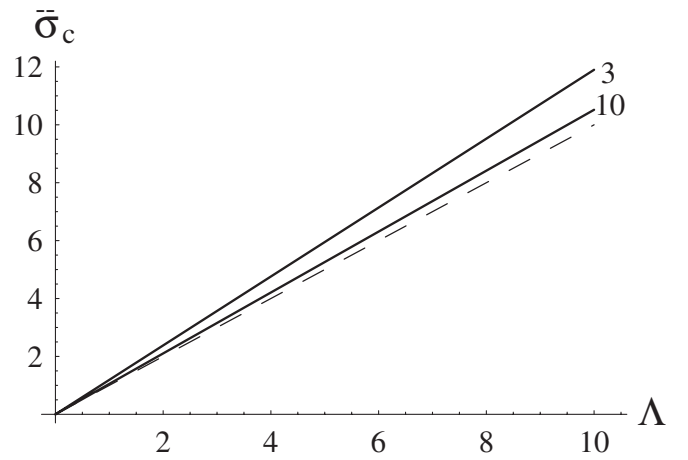


FIG. 3. The dimensionless minimum $\bar{\sigma}_c$ (in units of Λ) as a function of Λ for $T = \mu = 0$. The dashed line represents the $N \rightarrow \infty$ result, while the continuous lines were produced by the OPT-PMS at order δ . The numbers beside the curves identify the value of N for each case.

It is instructive to recall a similar result for the $d = 2$ where the large- N result is $\bar{\sigma}_c^N(\lambda) = M \exp(-\pi/\lambda)$ [24], while the OPT result is $\bar{\sigma}_c^{\delta^1} = \bar{\sigma}_c^N(\lambda^*)/[1 - 1/(2N)]$, where $\lambda^* = \lambda[1 - 1/(2N)]$ [13]. The same happens here except that we have a factor 4 inside the function dependent on N , Eq. (4.13), instead of a factor 2 found in the $d = 2$ case. This is because of the 4×4 Dirac matrices considered in the three dimensional problem here. Thus, we have $\bar{\sigma}_c^{\delta^1} = \bar{\sigma}_c^N(\lambda^*)/[1 - 1/(4N)]$, recalling that $\bar{\sigma}_c^N(\lambda) = \Lambda = \pi/|\lambda|$. Finally, when we evaluate the thermodynamical potential in the sequel, it will be useful to consider the optimized free energy at its minimum, $\sigma_c = \bar{\sigma}_c$, which is given by

$$\frac{V_{\text{eff}}(\bar{\eta}, \bar{\sigma}_c)}{N} = -\frac{\Lambda^3}{6\pi \mathcal{F}(N)^3}. \quad (4.15)$$

B. The $T \neq 0$ and $\mu = 0$ case

Next, let us consider the case $T \neq 0$ and $\mu = 0$ when the free energy can be written, using again $\lambda \rightarrow -\lambda$ and $\Lambda = \pi/|\lambda|$, as

$$\frac{V_{\text{eff}}^{\delta^1}(\eta, \sigma_c, T)}{N} = -\delta \Lambda \frac{\sigma_c^2}{2\pi} + \frac{\eta^3}{3\pi} \\ + \frac{2}{\pi} [\eta T^2 \text{Li}_2(-e^{-\eta/T}) + T^3 \text{Li}_3(-e^{-\eta/T})] \\ - \frac{\eta}{\pi} (\eta - \sigma_c) [\eta + 2T \ln(1 + e^{-\eta/T})] \\ - \delta \frac{\eta^2}{8\pi N \Lambda} [\eta + 2T \ln(1 + e^{-\eta/T})]^2, \quad (4.16)$$

where we have considered again the case $\sigma_c > 0$ and

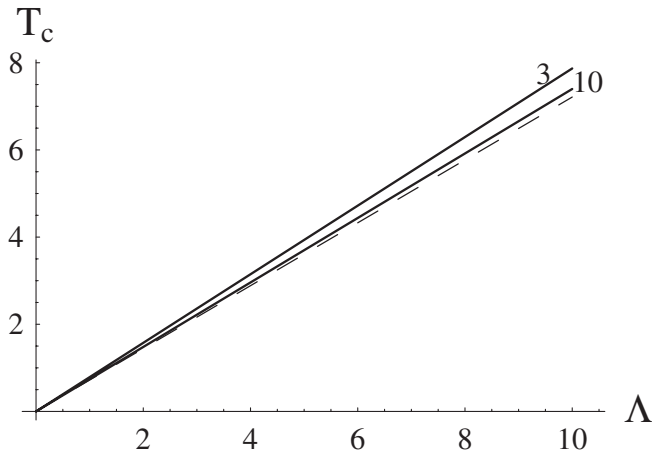


FIG. 4. The OPT critical temperature (at $\mu = 0$ and in units of Λ) as a function of Λ . The dashed line represents the $N \rightarrow \infty$ result, while the continuous lines were produced by the OPT-PMS procedure at order δ . The numbers beside the curves identify the value of N for each case.

$\eta > 0$. From the result given in Eq. (4.4), $\bar{\eta} = \sigma_c + \Sigma_a(\bar{\eta}, T, \mu = 0)$, we immediately obtain the self-consistent temperature dependent relation

$$\bar{\eta} = \sigma_c - \frac{\bar{\eta}}{4N\Lambda} [\bar{\eta} + 2T \ln(1 + e^{-\bar{\eta}/T})]. \quad (4.17)$$

It is a simple matter to apply $dV_{\text{eff}}/d\sigma_c = 0$ at $\sigma_c = \bar{\sigma}_c$ to Eq. (4.16) to obtain

$$\bar{\sigma}_c = \frac{\eta}{\Lambda} [\eta + 2T \ln(1 + e^{-\eta/T})], \quad (4.18)$$

which can be used in Eq. (4.17) to yield $\bar{\eta} = \bar{\sigma} \mathcal{F}(N)$ that, when inserted into Eq. (4.18), allows us to study the thermal behavior of the order parameter ($\bar{\sigma}_c(T)$) via the extremum of $V_{\text{eff}}^{\delta^1}(\eta, \sigma_c, T)$, given by [18]

$$\bar{\sigma}_c(T) \mathcal{F}(N) = \frac{\Lambda}{\mathcal{F}(N)} - 2T \ln[1 + e^{-\bar{\sigma}_c(T) \mathcal{F}(N)/T}]. \quad (4.19)$$

From the above equation one retrieves the result $\bar{\sigma}_c(0) = \Lambda \mathcal{F}(N)^{-2}$, as obtained in the previous subsection. The critical temperature T_c for chiral symmetry restoration is obtained by requiring that $\bar{\sigma}_c(T = T_c) = 0$, which gives

$$\begin{aligned} \frac{V_{\text{eff}}^{\delta^1}(\eta, \sigma_c, \mu, T = 0)}{N} &= \delta \frac{\sigma_c^2}{2\lambda} + \frac{|\eta|^3}{3\pi} - \frac{\delta(\eta - \sigma_c)\eta}{\pi} |\eta| + \frac{\delta\lambda\eta^4}{2(2\pi)^2 N} \\ &+ \left[\frac{1}{2\pi} \left(-\frac{2}{3} |\eta|^3 + |\mu|\eta^2 - \frac{|\mu|^3}{3} \right) - \frac{\delta\eta(\eta - \sigma_c)}{\pi} (|\mu| - |\eta|) + \frac{\delta\lambda\eta^2}{2(2\pi)^2 N} (\mu^2 - \eta^2) \right. \\ &\left. + \frac{\delta\lambda}{8(2\pi)^2 N} (\eta^2 - \mu^2)^2 \right] \theta(|\mu| - |\eta|). \end{aligned} \quad (4.21)$$

For $\mu = 0$, obviously, Eq. (4.21) reduces to Eq. (4.8).

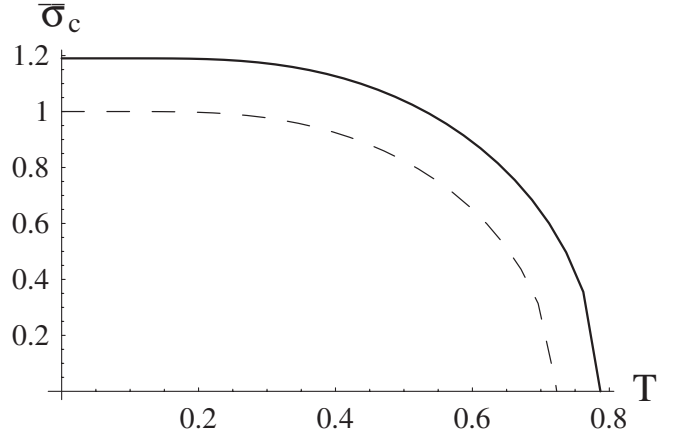


FIG. 5. The large- N (dashed line) and the OPT (continuous line) predictions for $\bar{\sigma}_c(T)$ at $N = 3$. All quantities are in units of Λ . The figure displays a continuous, second order transition line.

the result

$$T_c^{\delta^1} = \frac{\Lambda}{2 \ln 2} \frac{1}{\mathcal{F}(N)}. \quad (4.20)$$

This analytical result is shown in Fig. 4. Note that a numerical application of the PMS to the OPT effective potential, using Eqs. (4.7) and (4.16), exactly reproduces the analytical result Eq. (4.20). Recall the similarity with the $d = 2$ case [13], where the LDE result was obtained from the large N result by the replacement $\lambda \rightarrow \lambda^* = \lambda[1 - 1/(2N)]$, just the same as in obtaining the scalar field VEV, as discussed in the previous subsection.

Note also that, contrary to the $d = 2$ case, our prediction for T_c is always greater (for finite N) than the large- N prediction. The transition is found to be of the second kind, as illustrated by Fig. 5.

C. The $T = 0$ and $\mu \neq 0$ case

Let us now consider the case $T = 0$ and $\mu \neq 0$. From the general expression of the effective potential at the first OPT order, Eq. (3.10), and using the $T \rightarrow 0$ results shown in Eqs. (3.16), (3.17), (3.18), and (3.19), we find that the chemical potential dependent effective potential is given by

To evaluate the critical value μ_c for chiral symmetry restoration, it is sufficient to compare the values of the effective potential at the minimum $V_{\text{eff}}(\bar{\sigma}_c, T = 0)$ with its value for $\mu \neq 0$ for $\bar{\sigma}_c = 0$. This is from the same line of reasoning employed in the $d = 2$ case discussed in Ref. [13]. In this case, we obtain the point where the two minima of the effective potential, at $\bar{\sigma}_c = 0$ and at $\bar{\sigma}_c \neq 0$ and $\mu = \mu_c$, coincide, i.e., there is a value μ_c which satisfies

$$V_{\text{eff}}^{\delta_1}(\bar{\sigma} = 0, \mu = \mu_c, T = 0) = V_{\text{eff}}^{\delta_1}(\bar{\sigma}_c, \mu = 0, T = 0). \quad (4.22)$$

It is a simple algebraic exercise to calculate both members of this equality. We first obtain from Eq. (4.21) that

$$\frac{V_{\text{eff}}^{\delta_1}(\bar{\sigma} = 0, \mu_c, T = 0)}{N} = -\frac{1}{6\pi} |\mu_c|^3 \left(1 - 3 \frac{\lambda}{16\pi N} |\mu_c| \right). \quad (4.23)$$

Then, to evaluate the right-hand side of Eq. (4.22) we use Eq. (4.8) together with the relation between $\bar{\sigma}_c$ and $\bar{\eta}$ in Eq. (4.12), i.e., $\bar{\sigma}_c = \bar{\eta}/[\mathcal{F}(N)]$, which gives

$$\begin{aligned} \frac{V_{\text{eff}}^{\delta_1}(\bar{\sigma}_c, \mu = 0, T = 0)}{N} &= |\bar{\eta}|^3 \left(\frac{1}{2\mathcal{F}(N)} - \frac{2}{3} + \frac{\lambda \bar{\eta}}{8\pi N} \right) \\ &= -\frac{|\bar{\eta}|^3}{6\pi}, \end{aligned} \quad (4.24)$$

where the last simplification arises from using the definition of $\mathcal{F}(N)$, Eq. (4.13), and noting that $\bar{\eta} = -\pi/[\lambda \mathcal{F}(N)]$. Note thus that $V_{\text{eff}}^{\delta_1}(\bar{\sigma}_c, \mu = T = 0)$ has formally the same simple expression as the leading order one, except of course that it includes nontrivial $1/N$ corrections via the explicit expression of $\bar{\eta}$. Now we may compare Eqs. (4.23) and (4.24) to finally extract μ_c [18],

$$|\mu_c| = \frac{\Lambda}{\mathcal{F}(N)} \left(1 + \frac{3}{16N} \frac{|\mu_c|}{\Lambda} \right)^{-1/3}, \quad (4.25)$$

where we used again $\Lambda = \pi/|\lambda|$. For $N = 3$, we find from Eq. (4.25) the solution

$$\frac{\mu_c}{\Lambda} \simeq 1.06767, \quad (4.26)$$

which agrees with the numerical results obtained in the next subsection.

D. The $T \neq 0$ and $\mu \neq 0$ case

Finally, turning now to the case of both finite temperature and finite chemical potential, we obtain the full phase diagram of the three dimensional GN model. The numerical application of the PMS shows how the phase diagram is qualitatively and quantitatively affected by finite N corrections. Figure 6 shows the situation for $N = 3$. The CSB region is augmented with respect to the large- N predictions, when expressed in units of our reference scale $\Lambda \equiv$

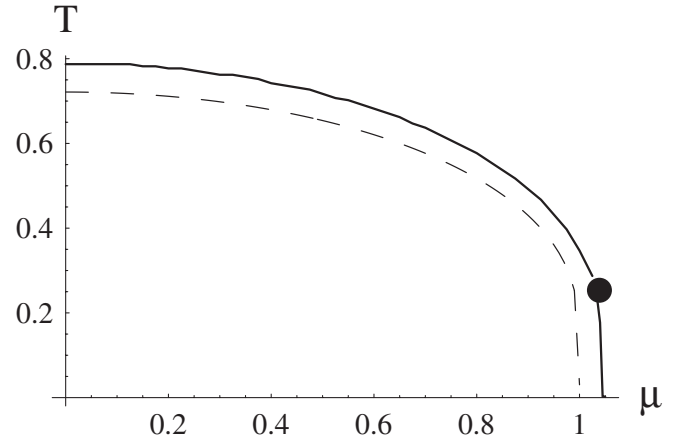


FIG. 6. The large- N (dashed line) and OPT (continuous line) predictions for the phase diagram at $N = 3$. All quantities are in units of Λ . The black dot indicates the position of a tricritical point, located at $T_{\text{tr}} \simeq 0.251$ and $\mu_{\text{tr}} \simeq 1.029$. Below this point the transition is of the first kind while above the point it is of the second kind.

$\pi/|\lambda|$. This is clear also from our results for $\bar{\sigma}_c$, T_c , and μ_c . This appears at first sight in contrast with the lattice results [12], which show a decreasing of the CSB region at finite N , as compared to the large- N results. However, within our approximation, the increase of the size of the CSB region is rather small, being about 5% for $N = 3$, while the increase would be of only about 2% for the $N = 12$ case considered in Ref. [12], which in turn predicts a decrease of about 10%. One should moreover note that in Ref. [12] the authors present their results for the phase diagram with quantities normalized by the scalar vacuum expectation value obtained from the lattice simulations. In our case it means that from Eqs. (4.14), (4.20), and (4.25), taking $N = 3$ for instance, $T_c/\bar{\sigma}_c \simeq 0.661$ and $\mu_c/\bar{\sigma}_c \simeq 0.897$, while for $N = 12$, $T_c/\bar{\sigma}_c \simeq 0.707$, and $\mu_c/\bar{\sigma}_c \simeq 0.976$, which approximately agrees with the results presented in Ref. [12] within their level of precision. Note also that our results agree reasonably with recent analysis of the $2 + 1$ GN model from exact renormalization group methods [29] (at least within the errors quoted there, and for the case of vanishing wave function of the auxiliary scalar field, which is the appropriate comparison to our analysis). Thus the reduction or increase with respect to large N results appears to be just a matter of scaling. In the present work we consider the scale defined as Λ (the vacuum expectation value of the scalar field at large- N) as more appropriate to present the results. In a previous work [13], we considered the same model but in $1 + 1$ dimensions using exactly the same approximation. There, our result for the phase diagram showed a drastic change concerning the size of the CSB which was about 30% smaller than the one produced by the large- N approximation for $N = 3$. Now, in $2 + 1$ dimensions, it turns out that the CSB region predicted by the OPT is very close to the one predicted by the

large- N approximation. In summary, in the fixed normalization scale used (Λ), it looks like the OPT predicts a drastic decrease in the size of the CSB region in $1 + 1$ dimensions whereas in $2 + 1$ dimensions it seems to support, at least at lowest OPT order, the CSB size (as well as the numerical values of $\bar{\sigma}_c$, T_c , and μ_c) predicted at large- N . We shall see in the next section that a partial investigation of higher OPT order corrections (for $T = \mu = 0$) indicates a good stability of these first order results. On the other hand, the nature of the transition line predicted at large- N in $1 + 1$ dimensions is unaffected by the OPT at order δ while it drastically changes in $2 + 1$ dimensions, as we now start to discuss.

Concerning the nature of the transition lines shown in Fig. 6, recall that the large- N approximation predicts that it is of the second kind everywhere, except at $T = 0$ where it suddenly becomes of the first kind at a critical value of $\mu = \mu_c^N = \Lambda$. Using lattice Monte Carlo simulations for the GN model, Kogut and Strouthos [11] concluded that, for $N = 4$, there should be a tricritical point on the section of the phase boundary defined by $T/T_c^N \leq 0.230$ and $\mu/\mu_c^N \geq 0.970$. Our evaluations predict that the observed first order transition at $T = 0$ spreads out through the transition line until it reaches a tricritical point at $T_{\text{tr}} \approx 0.251\Lambda$ and $\mu_{\text{tr}} \approx 1.029\Lambda$ (for $N = 3$).

Figure 7 shows an envelope of curves that displays how the abrupt first order transition at $T = 0$ becomes smoother as the temperature increases. One observes that the discontinuity gap becomes smaller as the temperature approaches the tricritical value, $T_{\text{tr}} = 0.251\Lambda$.

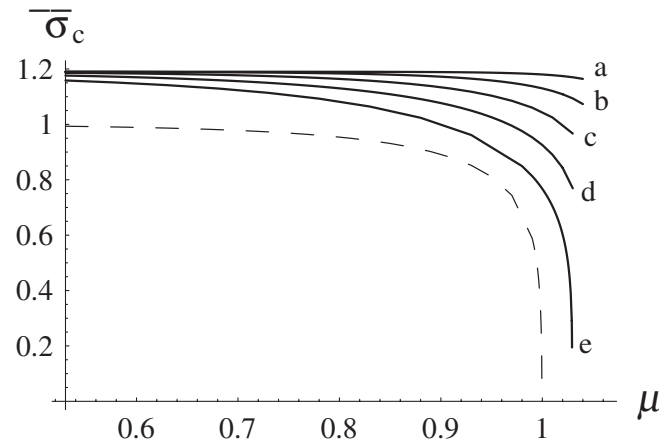


FIG. 7. The order parameter, $\bar{\sigma}_c$, as a function of μ for different temperatures. The continuous lines represent the OPT results for $N = 3$ and the labels on the figure represent the different temperatures: $T_a = 0.050$, $T_b = 0.100$, $T_c = 0.150$, $T_d = 0.200$ and $T_e = 0.250$. All these values are smaller than the tricritical value $T_{\text{tr}} = 0.251$ and the associated curves clearly display first order transitions. All quantities are given in units of Λ . For reference, the figure also shows the large- N result (dashed line) for $T = 0.150$.

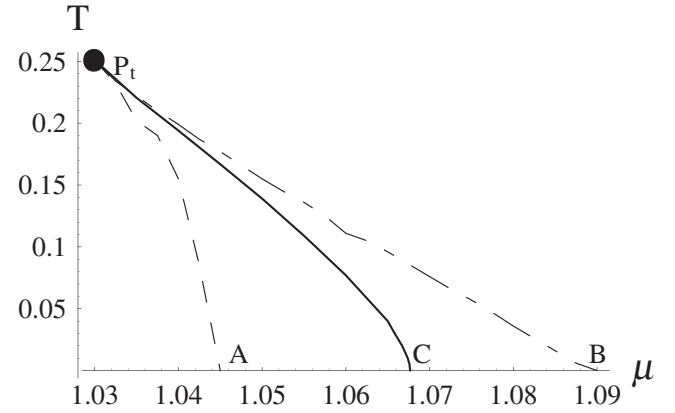


FIG. 8. Part of the phase diagram that corresponds to the metastable region (reproduced here from [18]). The dashed line joining points P_t and A refers to the development of a minimum at the origin. The continuous line linking the tricritical point to C ($T = 0$ and $\mu = \mu_c$) is the first order transition line, while the dot-dashed line joining P_t to B is the second metastability line and signals that the minima that occur away from the origin have disappeared.

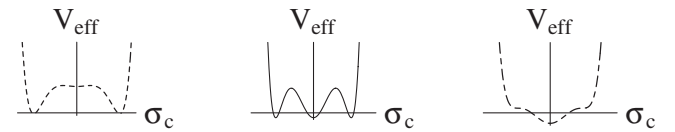


FIG. 9. The shape of the free energy corresponding to the metastable region. The left panel shows the situation corresponding to the dashed $P_t - A$ line shown in Fig. 8, while the middle and right panels correspond to lines $P_t - C$ and $P_t - B$, respectively.

It is also important to analyze the occurrence of metastability lines related to the first order transition line ($T < T_{\text{tr}}$) in Fig. 6. With this aim we offer Fig. 8, where the dashed line joining the tricritical point, P_t , to point A corresponds to the appearance of a minimum at $\sigma_c = 0$, whereas the continuous line joining points P_t and C refers to the first order transition line. Finally, the dot-dashed line joining points P_t and B refers to the vanishing of the minima that occurs away from the origin. It is important to note how small the metastable region $A - P_t - B$ is. As a matter of fact, point A occurs at a value of μ which is about 2% smaller than μ_c , whereas B occurs at a value which is about 3% greater than μ_c . In $d = 2$ these values are of about 30% (see Ref. [8]).

The reader may visualize the three situations shown in Fig. 8 by examining the form of the free energy shown in Fig. 9.

V. THE LIQUID-GAS PHASE

We are now in position to perform a more physical interpretation of our results by examining other relevant

thermodynamical quantities. The thermodynamical potential, $\Omega(\mu, T)$, for instance, is related to the free energy at its minimum, $\sigma_c = \bar{\sigma}_c$. It is given by

$$\Omega(\mu, T) = V_{\text{eff}}(\bar{\eta}, \bar{\sigma}_c, \mu, T). \quad (5.1)$$

Note that we have defined this quantity in terms of the *optimized* free energy. This is an important remark because we are considering different physical quantities and one could wonder which one to optimize. Here, our choice is to optimize the free energy since all other thermodynamical quantities may be obtained from it. It is usual to normalize the thermodynamical potential by subtracting a “bag” term, \mathcal{B} , given by $\mathcal{B} = \Omega(0, 0)$, so that the pressure as well as the energy density vanish at $T = 0$ and $\mu = 0$. In view of Eq. (4.15) the bag term is simply given by

$$\mathcal{B} = -\frac{\Lambda^3}{6\pi\mathcal{F}(N)^3}. \quad (5.2)$$

Then, the *normalized* thermodynamical potential is just $\Omega_N(\mu, T) = \Omega(\mu, T) - \mathcal{B}$. At the same time, the (normalized) pressure is given by $P(\mu, T) = -\Omega_N(\mu, T)$ from which one may obtain the density

$$\rho = \frac{\partial P}{\partial \mu}, \quad (5.3)$$

and the entropy density

$$\mathcal{S} = \frac{\partial P}{\partial T}. \quad (5.4)$$

Finally, the (normalized) energy density is given by $\mathcal{E} = -P + T\mathcal{S} + \mu\rho$. Recalling that, due to the gap equation, $\partial P/\partial \bar{\sigma}_c = 0$ and that, due to the PMS equation, $\partial P/\partial \bar{\eta} = 0$, one obtains the density

$$\begin{aligned} \rho = & -\frac{\bar{\eta}T^2}{\pi}I_{1,\mu} - \frac{T^3}{\pi}I_{2,\mu} + \frac{(\bar{\eta} - \bar{\sigma}_c)\bar{\eta}}{\pi}TI_{3,\mu} \\ & - \frac{\lambda\bar{\eta}^2}{(2\pi)^2N}T(\bar{\eta} + TI_3)I_{3,\mu} - \frac{\lambda T^4}{(2\pi)^2N}I_4I_{4,\mu}, \end{aligned} \quad (5.5)$$

where $I_{i,\mu} \equiv \partial I_i/\partial \mu$, and $I_i, i = 1, \dots, 4$, are given by the function in Eqs. (3.12), (3.13), (3.14), and (3.15). At the same time one obtains that the entropy density is given by

$$\begin{aligned} \mathcal{S} = & -2\frac{\bar{\eta}T}{\pi}I_1 - \frac{\bar{\eta}T^2}{\pi}I_{1,T} - 3\frac{T^2}{\pi}I_2 - \frac{T^3}{\pi}I_{2,T} \\ & + \frac{(\bar{\eta} - \bar{\sigma}_c)\bar{\eta}}{\pi}I_3 + \frac{(\bar{\eta} - \bar{\sigma}_c)\bar{\eta}}{\pi}TI_{3,T} \\ & - \frac{\lambda\bar{\eta}^2}{(2\pi)^2N}(\bar{\eta} + TI_3)(I_3 + TI_{3,T}) \\ & - \frac{\lambda T^3}{(2\pi)^2N}(2I_4^2 + TI_{4,T}), \end{aligned} \quad (5.6)$$

where $I_{i,T} \equiv \partial I_i/\partial T$.

Having all the above quantities, we can now analyze, for instance, the phase diagram in the physically more acces-

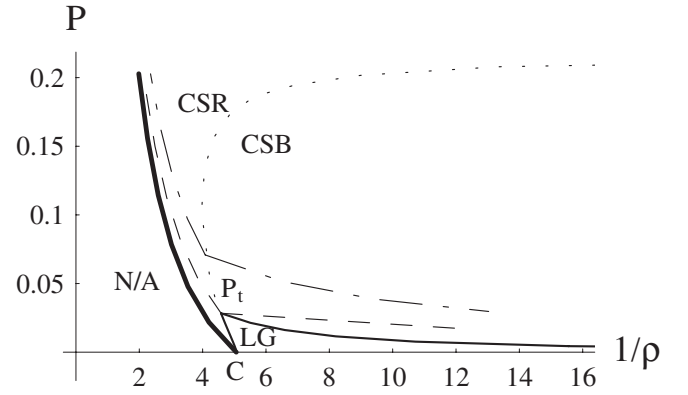


FIG. 10. The phase diagram in the $P - 1/\rho$ plane for $N = 3$. The thick continuous line is the $T = 0$ isotherm which limits the region accessible to the system. The region labeled by N/A is not accessible. The dotted line is the mapping of the second order transition line. The chiral symmetric region (CSR) corresponds to the liquid phase while the region where chiral symmetry is broken (CSB) corresponds to the gas phase. The LG region starting at the tricritical point, P_t , is limited by first order transition lines and corresponds to the mixed liquid-gas phase. Point C ($P = 0$ and $\rho \approx 0.197\Lambda^2$) corresponds to $T = 0$, $\mu = \mu_c$. The isotherm represented by the dashed line corresponds to the tricritical temperature, $T_{\text{cr}} = 0.251\Lambda$ while the dot-dashed line represents the isotherm corresponding to $T = 0.397\Lambda$. The pressure, P , is in units of Λ^3 while the density, ρ , is given in units of Λ^2 .

sible $P - 1/\rho$ plane as shown by Fig. 10. This figure displays one of our most important results which indicates that a mixed liquid-gas phase, previously unknown to exist within this model, develops at low pressure values. Three isotherms are shown, and the one corresponding to $T = 0$ defines the edge of the region accessible to the system. The dotted line above the tricritical point is just the mapping of the corresponding second order transition line in the $T - \mu$ plane. Note that in the $P - 1/\rho$ plane the first order transition line displayed in the $T - \mu$ plane (corresponding to $T < T_{\text{cr}}$) splits in two parts corresponding to the value of the density at the two degenerate minima which produce identical pressure values. Not being able to determine the existence of the mixed phase, Kogut and Strouthos argued that the liquid-gas transition was either (i) extremely weak, (ii) very close to the chiral transition, or (iii) not realized in this model [11]. Our result shown in Fig. 10 suggests that their second hypothesis was the correct one. Moreover, these authors had used $N = 4$; that was the smallest number allowed by the hybrid Monte Carlo algorithm used in their simulations. With this number the tricritical point appears at an even lower value of P (actually, for $N \rightarrow \infty$ it happens at $P = 0$) and was consequently harder to be detected within their approximation.

Figure 11 shows a detailed view of the liquid-gas phase seen in Fig. 10 displaying how an isotherm whose temperature is smaller than the tricritical value crosses the mixed phase region. The horizontal line in the “coexis-

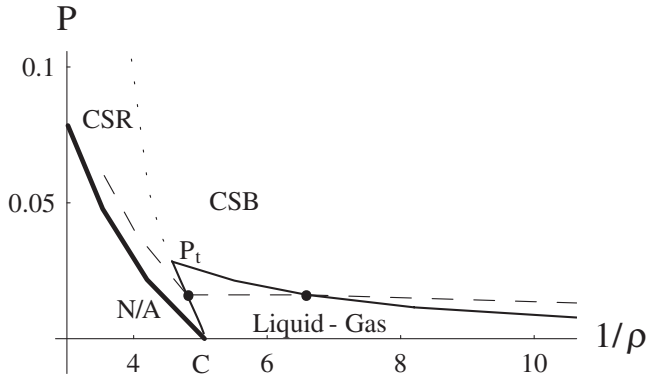


FIG. 11. Detail of the liquid-gas phase in the $P - 1/\rho$ plane for $N = 3$. The isotherm represented by the dashed line corresponds to a temperature $T = 0.194\Lambda$ that is smaller than the tricritical temperature, $T_{\text{tr}} = 0.251\Lambda$. The two dots are joined by a straight line in a Maxwell construction. The pressure, P , is in units of Λ^3 while the density, ρ , is given in units of Λ^2 .

tence” region was drawn by connecting the value of the pressure at the boundaries, corresponding to “mixed” states. This picture observes the Maxwell construction which derives from the equality of the chemical potentials at the edge of the two phases.

Figure 12 shows \mathcal{E}/T^3 and P/T^3 as functions of the temperature for $\mu = 0$. Note that for high temperatures $\mathcal{E}/T^3 \rightarrow -3\zeta(3)/\pi \simeq 1.14$, while $P/T^3 \rightarrow -3\zeta(3)/(2\pi) \simeq 0.57$ (where $\zeta(3) \simeq 1.202$), as one can guess by looking at the equations for \mathcal{E} and P at $\mu = 0$. In those high temperature regimes ($T > T_c$), we have $\bar{\sigma}_c = 0$ and $\bar{\eta} \rightarrow 0$. At high temperatures both curves are symmetrical with respect to the numerical value ~ 0.85 .

Let us now check for the presence of latent heat, which is inherent to first order phase transitions. We do this by examining the energy density as a function of the temperature. For this, one chooses a value of μ that corresponds to the first order transition, like, for example, any μ such that

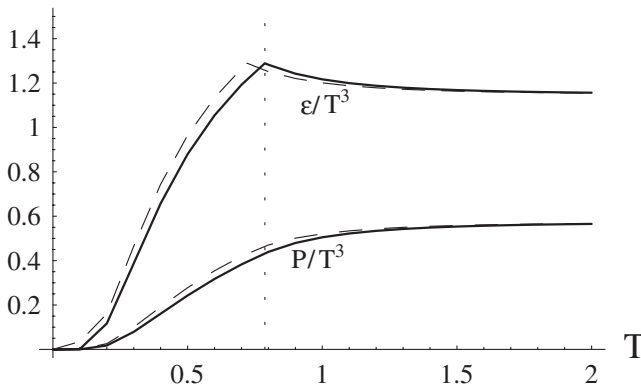


FIG. 12. The dimensionless quantities \mathcal{E}/T^3 and P/T^3 as functions of the temperature for $\mu = 0$. The continuous lines are the OPT results for $N = 3$, while the dashed lines represent the large- N results. The vertical dotted line is the OPT critical temperature for $N = 3$.

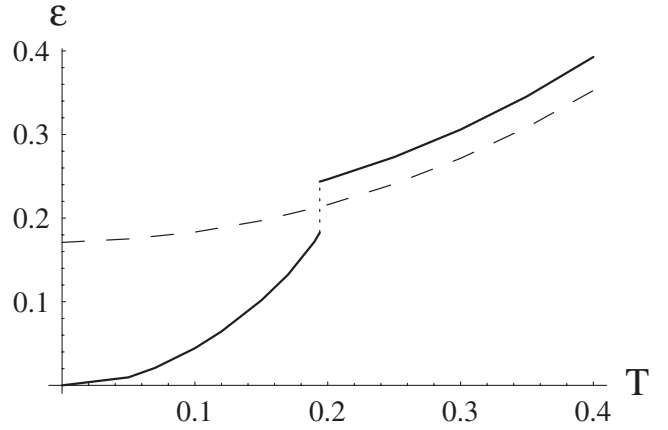


FIG. 13. The energy density, \mathcal{E} , as a function of the temperature for $\mu = 1.040 > \mu_{\text{tr}} = 1.029$ (for $N = 3$). Both quantities are in units of Λ . The continuous line is the OPT result and shows the presence of latent heat signaled by the discontinuity at $T_c(\mu = 1.040\Lambda) = 0.194\Lambda$. The large- N result is represented by the dashed line and the discontinuity happens at $T = 0$. Both \mathcal{E} and T are in units of Λ .

$\mu_c > \mu > \mu_{\text{tr}}$. Recall that for the case $N = 3$, $\mu_{\text{tr}} = 1.029\Lambda$ and $\mu_c = 1.067\Lambda$, so we choose, without loss of generality, the value $\mu = 1.040\Lambda$. One then expects to see a discontinuity in the line corresponding to $\mathcal{E}(T)$ at $T = T_c(\mu = 1.040\Lambda) = 0.194\Lambda$. This is indeed the case as shown in Fig. 13. The same figure shows the large- N result, where the discontinuity happens only at $T = 0$, which can be understood by recalling that within this approximation the first order phase transition happens only at the point $T = 0$ and $\mu = 1.000\Lambda$.

VI. ORDER δ^2 RESULTS AT $T = 0$ AND $\mu = 0$

Let us now investigate the order δ^2 contributions that are given by the three-loop graphs shown in Fig. 2. Actually, a complete evaluation of these graphs at finite T and μ turns out to be very cumbersome, so we shall restrict ourselves in the present work to the $T = 0$ and $\mu = 0$ case which is more tractable. This will at least allow us to have a reasonable quantitative estimate of the expected higher order corrections to our previous order δ results. We plan to tackle the calculation of the full T and μ dependence in a future work.

A. The order δ^2 three-loop contribution to the free energy

The total order δ^2 three-loop contribution can be easily extracted from Ref. [28] and reads

$$\frac{\Delta V_{\text{eff}}^{(b,c,d)}}{N} = -\frac{i}{4N} \int \frac{d^d p}{(2\pi)^d} \times \text{tr} \left[\frac{\Sigma_b(p, \eta) + \Sigma_c(p, \eta) + \Sigma_d(p, \eta)}{p - \eta + i\epsilon} \right], \quad (6.1)$$

where $\Sigma_i(p, \eta)$, $i = b, c, d$, correspond to panels (b), (c), and (d) (second, third, and fourth diagrams, respectively) in Fig. 1.

The most complicated contributions arise from the first and second terms of the above equation (or equivalently corresponding to the third and fourth graphs of Fig. 2) since in this case the self-energies depend on the momentum p . After taking the traces, etc., and using dimensional regularization with $d = 3 - \epsilon$, the corresponding integral to be evaluated reads

$$\begin{aligned} \frac{V_{\text{eff}}^{(b,c)}}{N} &= \delta^2 \lambda^2 \frac{4}{N} \left(1 - \frac{1}{4N}\right) \left(\frac{e^{\gamma_E} M^2}{4\pi}\right)^{3\epsilon/2} i \int \frac{d^d p}{(2\pi)^d} \\ &\times \left\{ i \int \frac{d^d k}{(2\pi)^d} \frac{k^2 + pk + \eta^2}{(k^2 - \eta^2)[(p+k)^2 - \eta^2]} \right\}^2. \end{aligned} \quad (6.2)$$

Introducing next appropriate Feynman parameters to disentangle the different momenta integrations, we obtain the following expression

$$\begin{aligned} \frac{\Delta V_{\text{eff}}^{(b,c)}}{N} &= -\delta^2 \lambda^2 \frac{\eta^5}{(4\pi)^3 (4\pi)^{3/2}} \frac{4}{N} \left(1 - \frac{1}{4N}\right) \Gamma\left(-\frac{5}{2} + \frac{3\epsilon}{2}\right) \\ &\times (2 - \epsilon)^2 \left(\frac{e^{\gamma_E} M^2}{\eta^2}\right)^{3\epsilon/2} \int_0^1 d\alpha d\beta d\gamma g(\gamma) \\ &\times H(\alpha, \beta, \gamma), \end{aligned} \quad (6.3)$$

where M is the arbitrary $\overline{\text{MS}}$ renormalization scale,

$$g(\gamma) = [\gamma(1 - \gamma)]^{-3/2 + \epsilon/2}, \quad (6.4)$$

and

$$H(\alpha, \beta, \gamma) = [\gamma\alpha(1 - \alpha) + (1 - \gamma)\beta(1 - \beta)]^{-3/2 + \epsilon/2}. \quad (6.5)$$

The evaluation of the final integrals over Feynman parameters in Eq. (6.3) is rather technical and details of this calculation are left to Appendix B. One arrives at the final result for the third and fourth three-loop diagrams of Fig. 2 as given by

$$\begin{aligned} \frac{\Delta V_{\text{eff}}^{(b,c)}}{N} &= \delta^2 \lambda^2 \frac{\eta^5}{30\pi^3} \frac{4}{N} \left(1 - \frac{1}{4N}\right) \\ &\times \left[\frac{1}{\epsilon} + \frac{41}{10} - 4 \ln 2 - \frac{X}{2} - 3 \ln \frac{\eta}{M} \right], \end{aligned} \quad (6.6)$$

where $X \sim 1.63669$ is a numerical constant obtained from the integrations. Next, the self-energy entering the last term of Eq. (6.1), corresponding to the last diagram shown in Fig. 1, that leads to the contribution to V_{eff} shown by the fifth diagram in Fig. 2 is a tadpole-like graph that can be easily evaluated with the standard Feynman rules. It is finite and gives the contribution

$$\frac{\Delta V_{\text{eff}}^{(d)}}{N} = -\delta^2 \lambda^2 \frac{\eta^5}{2N^2 (4\pi)^3}. \quad (6.7)$$

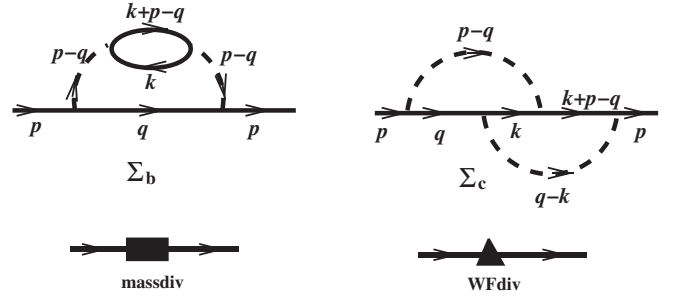


FIG. 14. Momentum-dependent two-loop graphs contributing to the fermionic self-energy to order δ^2 . $\Sigma_b(p)$ is of order $1/N$ while $\Sigma_c(p)$ contributes with $1/N^2$. The other two graphs represent the mass and the wave function counterterms as indicated in the figure.

At the three-loop order, the free energy contains divergent terms that lead to the $1/\epsilon$ term shown in Eq. (6.6). The renormalization is performed as usual, by introducing the appropriate counterterms (mass, wave function, etc.). Actually the perturbative two-loop fermion self-energy in Fig. 14 exhibits divergent terms of nonrenormalizable kind, with higher power of momentum dependence, as expected since the model is not perturbatively renormalizable. Although it would not be a problem in principle to treat those new divergences with appropriate counterterms, similarly to what is done in other effective theories, it turns out that these nonrenormalizable counterterms do not contribute to the three-loop free energy in dimensional regularization, so that only standard mass, wave function and vacuum counterterms are needed in practice to render the effective potential at $\mathcal{O}(\delta^2)$ finite. Thus the renormalization as performed in the $\overline{\text{MS}}$ scheme after dimensional regularization does not introduce new parameters at the three-loop order, for the quantities we are interested in. The arbitrariness of the final physical result for the three-loop effective potential simply takes the standard form of a (logarithmic) dependence on an arbitrary renormalization scale. The details of the calculation of these counterterm contributions are discussed in Appendix C. Now, by adding all contributions, including the finite ones arising from the counterterms (see Appendix C), the renormalized three-loop effective potential can be cast into the form

$$\begin{aligned} \frac{\Delta V_{\text{eff,ren}}^{(b,c,d)}}{N} &= \delta^2 \lambda^2 \frac{\eta^5}{\pi^3} \left[\frac{4}{N} \left(1 - \frac{1}{4N}\right) \right. \\ &\times \left. \left(\frac{3}{25} - \frac{X + 7 \ln 2}{60} - \frac{1}{12} \ln \frac{\eta}{M} \right) - \frac{1}{128N^2} \right]. \end{aligned} \quad (6.8)$$

B. Optimization results at $T = 0$ and $\mu = 0$ at order δ^2

From the result for the $\mathcal{O}(\lambda^2 \delta^2)$ three-loop contribution, Eq. (6.8), we can now perform the δ expansion and PMS optimization at this next order, limited however here to the

special case $T = 0$ and $\mu = 0$. Following the same line of reasoning as in Sec. IVA, care is to be taken by noticing that other δ^2 terms are generated by the appropriate expansion of η^* , as defined in Eq. (3.5), within the first order $\mathcal{O}(\delta\lambda)$ terms. Explicitly, after having redefined $\lambda \rightarrow -\pi/\Lambda$ as previously, we arrive at the expression

$$\begin{aligned} \frac{V_{\text{eff}}^{\delta^2}(\eta, \sigma_c)}{N} = & -\delta \frac{\sigma_c^2 \Lambda}{2\pi} + \frac{\eta^3}{3\pi} - \delta \frac{\eta^2(\eta - \sigma_c)}{\pi} \\ & - \delta \frac{\eta^4}{8\pi N \Lambda} + \delta^2 \frac{\eta(\eta - \sigma_c)^2}{\pi} \\ & + \delta^2 \frac{\eta^3(\eta - \sigma_c)}{2\pi N \Lambda} + \delta^2 \frac{\eta^5}{\Lambda^2 \pi} \left[\frac{4}{N} \left(1 - \frac{1}{4N} \right) \right. \\ & \left. \times \left(\frac{3}{25} - \frac{X + 7 \ln 2}{60} - \frac{1}{12} \ln \frac{\eta}{M} \right) - \frac{1}{128 N^2} \right]. \end{aligned} \quad (6.9)$$

The remaining is simply an algebraic exercise to apply the PMS procedure to Eq. (6.9). Similar to the first order case, the gap equation $dV_{\text{eff}}/d\sigma_c = 0$ at $\sigma_c = \bar{\sigma}_c$ defines $\bar{\sigma}_c$ as a function of $\bar{\eta}$, while the PMS equation $dV_{\text{eff}}/d\eta = 0$ at $\eta = \bar{\eta}$ gives a further relation between $\bar{\sigma}_c$ and $\bar{\eta}$. However, at this next order, both relations are more complicated; in particular, the PMS equation is nonlinear and involves a $\ln(\eta)$ term. It is most convenient to use the gap equation, which gives

$$\bar{\sigma}_c = \frac{\eta^2}{2\eta - \Lambda} \left(1 + \frac{\eta}{2N\Lambda} \right), \quad (6.10)$$

generalizing Eq. (4.10), at second δ order, into the PMS equation, which defines an equation depending only on $\bar{\eta}(N)$ (note that the dependence upon Λ can be simply factored out, e.g., by rescaling $\bar{\eta}$ in units of Λ). For instance, for the particular case $N = 3$, which is just sufficient for our illustration, one obtains the PMS equation as

$$\begin{aligned} \hat{\eta}^2 \left\{ -0.0217944(\hat{\eta} - 0.819029)(\hat{\eta} + 1.28009) \right. \\ \left. \times [3.48261 + \hat{\eta}(\hat{\eta} - 3.6924)] \right. \\ \left. - 0.162102 \left(\hat{\eta} - \frac{1}{2} \right) \hat{\eta}^2 \ln \frac{\hat{\eta} \Lambda}{M} \right\} = 0, \end{aligned} \quad (6.11)$$

where we have defined, for convenience, the dimensionless mass parameter $\hat{\eta} \equiv \eta/\Lambda$. Equation (6.11) can be solved numerically, to find a nontrivial value of $\bar{\eta}$. For this we have to set the arbitrary renormalization scale M in (6.11), originating from the logarithmic dependence in Eq. (6.9), to some appropriate value. A physically natural choice is to set $M = \Lambda$; that corresponds to the basic scale and scalar vacuum expectation value in the large- N limit. An interesting feature of the optimization result in the present case is that the presence of the $\ln(\eta)$ dependence in Eq. (6.11) largely reduces the number of optimized solutions (usually a drawback of the PMS). Indeed, one sees in Eq. (6.11) that, without the logarithmic term, four different nonzero

(real or complex) $\bar{\eta}$ solutions would occur.³ In contrast, we find here numerically a unique (real) solution (for $M = \Lambda$ and $N = 3$):

$$\bar{\eta} \simeq 0.867\Lambda. \quad (6.12)$$

Next, we can just plug in this result into Eq. (6.10), to obtain

$$\bar{\sigma}_c^{\delta^2} \simeq 1.1719\Lambda, \quad (6.13)$$

which appears to be very close to the first order result, $\bar{\sigma}_c^{\delta^1} \simeq 1.1901\Lambda$, obtained from Eq. (4.14) for $N = 3$. One may however question if this is an artifact of our choice of arbitrary renormalization scale $\Lambda = M$. Though this value of the scale appears to be very natural, it is easy to study the impact of varying it in a reasonable range around this value, like is sensible to do in similar renormalization scale dependence studies in other theories (and which give a rough estimate of higher order corrections). We can, e.g., vary M in the range $0.50\Lambda \leq M \leq 1.50\Lambda$, which correspondingly changes $\bar{\sigma}_c$ from values $1.16\Lambda \leq \bar{\sigma}_c \leq 1.38\Lambda$ (note that for M values too far apart from $M \sim \Lambda$, Eq. (6.11) has no real solutions). From this we conclude that the higher δ^2 order corrections for $T, \mu = 0$ to the previous analysis are quite small, though their scale dependence is apparent and can become non-negligible. Actually, it is clear that the scale dependence is essentially determined by the relative size of the $\ln(\eta/M)$ term with respect to constant terms in the optimization Eq. (6.11), which turns out to be moderate.⁴ On general grounds, renormalization scale dependence is expected to be rather pronounced at lowest loop orders and damped by higher order perturbative contributions [25]. But in our framework the three-loop expression, Eq. (6.8), is the very first perturbative order at which renormalization, and thus scale dependence, occur for the effective potential, so that the behavior is more similar to a one-loop quantity with respect to renormalization scale dependence. For the natural scale choice $M = \Lambda$, however, these second order corrections for $\bar{\sigma}_c$ value in Eq. (6.13) are very small, about only 1.5% of the first order value, so in other words the OPT expansion seems to converge rather quickly.

³One may wonder if the peculiar choice of the arbitrary scale $M = \bar{\eta}$, thus canceling the logarithmic term, would not reintroduce the PMS multisolution problem. But this gives no consistent optimal solutions since all other $\bar{\eta}$ solutions contradict this value of $\bar{\eta}$. This incidentally shows that Eq. (6.11) does not always have real solutions for any values of M .

⁴It is interesting to note also that from Eq. (6.10) $\bar{\sigma}_c(\eta)$ has a minimum, $\bar{\sigma}_c \sim 1.16\Lambda$, at $\eta \sim 0.94\Lambda$, independent of the scale M , thus $\bar{\sigma}_c$ cannot reach values below $\sim 1.16\Lambda$: when varying the scale M to values lower than Λ , the optimal solution $\bar{\eta}$ of Eq. (6.11) decreases, so that $\bar{\sigma}_c(\bar{\eta})$ will start to increase again. Also, the unwelcome singularity of $\bar{\sigma}_c$ for $\eta = \Lambda/2$, apparent in Eq. (6.10), is not a solution of Eq. (6.11), so this singular value is never reached by the consistent PMS optimal solution $\bar{\eta}$.

VII. CONCLUSIONS

In the present paper we have applied the alternative analytical nonperturbative optimized perturbation theory (OPT) approach, through which one can easily include finite N effects, to a four-fermion theory with discrete chiral symmetry represented by the massless Gross-Neveu model in $2 + 1$ dimensions. We have then evaluated the free energy, or effective potential, for the model at both finite temperature and finite chemical potential. The evaluation of the optimal value for this quantity has allowed us to derive and study in detail other thermodynamical quantities, such as the pressure, density, entropy, and energy density.

Our main results in this paper include the analytical derivation of expressions, going beyond the standard large- N results, for the scalar field vacuum expectation value, the critical temperature, and for critical chemical potential related to chiral symmetry breaking/restoration. We have also demonstrated the existence of a tricritical point, not seen in the large- N approximation, and the corresponding existence of a mixed chiral restored-broken phase in the system for finite values of chemical potential and temperature. Concerning the phase diagram we recall that in a lattice simulation, Kogut and Strouthos [11] have predicted the existence of a tricritical point in the $T - \mu$ plane that is missed by the large- N approximation. However, within the numerical precision of their simulations, those authors were unable to give its exact location. Here, we have not only confirmed the existence of such a point but have also demonstrated how it can be located for any value of N . The formalism employed in this work has allowed us to easily draw the first order transition line together with the metastability lines. This exercise showed that the metastable region is rather small which possibly explains why its observation was not possible in Refs. [11,12]. Going to the $P - 1/\rho$ plane has generated another important result for the GN3d model, namely, the prediction of a liquid-gas phase transition, so far unknown to exist in this model. All these results drastically change the large- N picture of the GN3d phase diagram in which only a “superconducting” phase and a “normal” phase appear [4]. Although in our study the complete T and μ dependence could only be studied at the first nontrivial order of the δ expansion, we were able to estimate the higher order δ^2 corrections at least at $T = 0$ and $\mu = 0$. These corrections turn out to be reasonably small (about only 1.5% for a natural choice of renormalization scale). This also indicates that all other OPT order δ^2 results are not expected to be too distant from the computed order δ results obtained for the GN3d model. So, we may argue that all our phase transition and thermodynamical results obtained in Secs. V and VI are likely to remain qualitatively unaltered by higher order corrections in this framework.

We notice that some of our quantitative results (most notably those displayed by Figs. 3 to 6) appear at first sight different from the overall behavior obtained with some Monte Carlo simulations [12] that predict a reduced size for the CSB region, while our results display an increase of the CSB region with respect to the large N (equivalently mean-field) results. As discussed previously, as far as we can compare this seems to be only an artifact of the different reference scales chosen to express the critical quantities (e.g., the authors of Ref. [12] express the phase diagram in terms of the scalar field vacuum expectation value, while we express all the relevant quantities in units of the fixed reference scale (Λ)). But we note also that even for our choice of reference scale the increase with respect the large- N results is rather very small. This is opposite to what is seen when the same approximation is applied to the $1 + 1$ dimensional GN case [13] where a large decrease of the CSB region is observed compared to the large- N (mean-field) results. In this respect, the OPT applied to the $2 + 1$ dimensional GN model leads to results closer to the mean-field approximation, though the character of the CSB/CSR transition line is qualitatively very different.

As usual, within the OPT, all the large- N results are exactly recovered from our expressions by taking the limit $N \rightarrow \infty$. In addition to the explicit thermodynamical analysis presented here, we have also shown in detail, in Appendices B and C, the renormalization of the effective potential up to $\mathcal{O}(\delta^2)$ in the OPT. A comparison to the case of renormalization within the $1/N$ expansion is also briefly provided. In the case of the main expressions derived in this work, all results to $\mathcal{O}(\delta)$ are shown to be finite within the dimensional regularization in the OPT. Divergences start to appear at second order. At this order the effective potential can be rendered completely finite just with standard counterterms. Possible extensions of the present work are presented in Ref. [18].

ACKNOWLEDGMENTS

M. B. P. and R. O. R. are partially supported by CNPq-Brazil. E. S. is partially supported by CAPES-Brazil. R. O. R. also acknowledges partial support from FAPERJ. J.-L. K. acknowledges partial support from UFSC.

APPENDIX A: SUMMING MATSUBARA FREQUENCIES AND RELATED FORMULAS

In this appendix we give the results for the main integrals and Matsubara sums appearing along the text. Following the general procedure for evaluating these sums [19] and using dimensional regularization in the $\overline{\text{MS}}$ scheme, the momentum space integrals are written as

$$\int \frac{d^d p}{(2\pi)^d} \rightarrow \left(\frac{e^{\gamma_E} M^2}{4\pi} \right)^{\epsilon/2} \int \frac{d^{d-1} p}{(2\pi)^{d-1}},$$

where $d = 3 - \epsilon$, M is an arbitrary mass scale, and $\gamma_E \simeq 0.5772$ is the Euler-Mascheroni constant.

For the general case of $T \neq 0$ and $\mu \neq 0$, we then obtain, for example, that

$$i \int_p^{(T)} \ln(P^2 - \eta^2 + i\epsilon) = \frac{|\eta|^3}{3\pi} + \frac{\eta}{\pi} T^2 \{ \text{Li}_2[-e^{-(|\eta|-|\mu|)/T}] + \text{Li}_2[-e^{-(|\eta|+|\mu|)/T}] \} \\ + \frac{T^3}{\pi} \{ \text{Li}_3[-e^{-(|\eta|-|\mu|)/T}] + \text{Li}_3[-e^{-(|\eta|+|\mu|)/T}] \}, \quad (\text{A1})$$

$$i \int_p^{(T)} \frac{1}{P^2 - \eta^2 + i\epsilon} = -\frac{T}{4\pi} \left\{ \frac{|\eta|}{T} + \ln[1 + e^{-(|\eta|-|\mu|)/T}] + \ln[1 + e^{-(|\eta|+|\mu|)/T}] \right\}, \quad (\text{A2})$$

$$i \int_p^{(T)} \frac{P_0^2}{P^2 - \eta^2 + i\epsilon} = -i \text{sgn}(\mu) \frac{T^2}{4\pi} \left\{ \frac{|\eta|}{T} \ln \left[\frac{1 + e^{(|\eta|+|\mu|)/T}}{1 + e^{(|\eta|-|\mu|)/T}} \right] + \text{Li}_2[-e^{(|\eta|+|\mu|)/T}] - \text{Li}_2[-e^{(|\eta|-|\mu|)/T}] \right\}, \quad (\text{A3})$$

where $\text{sgn}(\mu)$ is the sign function and $\text{Li}_\nu(z)$ is the polylogarithm function defined (for $\nu > 0$) as [30]

$$\text{Li}_\nu(z) = \sum_{k=1}^{\infty} \frac{z^k}{k^\nu}.$$

APPENDIX B: EVALUATION OF THREE-LOOP FREE ENERGY GRAPHS AT $T = 0$ AND $\mu = 0$.

In this appendix we give some technical details on the evaluation of the two complicated contributions to the three-loop free energy. These are the third and fourth graphs of Fig. 2 respectively, which give the expression Eq. (6.3). There are probably different ways to perform this integral. For convenience we choose to first integrate on the Feynman parameter γ , which can be done analytically, with the result:

$$\frac{\Delta V_{\text{eff}}^{(c,d)}}{N} = -\frac{4}{N} \left(1 - \frac{1}{4N} \right) \frac{\delta^2 \lambda^2 \eta^5}{(4\pi)^{9/2}} \left(\frac{e^{\gamma_E} M^2}{\eta^2} \right)^{3\epsilon/2} \\ \times \Gamma \left(-\frac{5}{2} + \frac{3\epsilon}{2} \right) (2 - \epsilon)^2 \frac{\Gamma^2(-\frac{1}{2} + \frac{\epsilon}{2})}{\Gamma(-1 + \epsilon)} \\ \times \int_0^1 d\alpha d\beta [\beta(1 - \beta)]_2^{-(3/2) + (\epsilon/2)} \\ \times F_1 \left[-\frac{1}{2} + \frac{\epsilon}{2}, \frac{3}{2} - \frac{\epsilon}{2}, -1 + \epsilon; 1 - z \right], \quad (\text{B1})$$

where ${}_2F_1$ is the hypergeometric function, with $z \equiv \alpha(1 - \alpha)/[\beta(1 - \beta)]$. Next we can use some well-known properties of the hypergeometric function [30], relating ${}_2F_1[\dots; z]$ to ${}_2F_1[\dots; 1 - z]$, and the power expansion in z of the hypergeometric function as

$${}_2F_1[p, q, r; z] = \sum_k \frac{(p)_k (q)_k}{(r)_k} \frac{z^k}{k!}, \quad (\text{B2})$$

where the $(p)_k$ etc. are binomial coefficients. These manipulations allow us to factorize explicitly the α and β integrals in the simple form

$$\int_0^1 dx x^p (1 - x)^q = \frac{\Gamma(1 + p)\Gamma(1 + q)}{\Gamma(2 + p + q)}, \quad (\text{B3})$$

with $x = \alpha, \beta$ with various possible values of p, q (which in the framework of dimensional regularization is valid for any values of p, q , since it will eventually exhibit the location of the different poles in $\epsilon = 0$). Next it is just a matter of systematic algebra, using for instance MATHEMATICA [31], to perform all these simple integrals, resumming the resulting power series to all orders, while picking up the divergent and finite pieces we need. Actually the divergent part occurs only in the first two terms of the power expansion in z of the ${}_2F_1$ function, which is simple to extract analytically. In contrast, the finite part results from contributions of all terms, which can be extracted numerically as the corresponding series converges quickly. Expanding all factors contained in Eq. (B1) for $\epsilon \rightarrow 0$ finally yields

$$\frac{\Delta V_{\text{eff}}^{(c,d)}}{N} = \delta^2 \lambda^2 \frac{\eta^5}{30\pi^3} \frac{4}{N} \left(1 - \frac{1}{4N} \right) \\ \times \left(\frac{1}{\epsilon} + \frac{41}{10} - 4 \ln 2 - \frac{X}{2} - 3 \ln \frac{\eta}{M} \right), \quad (\text{B4})$$

where $X \sim 1.63669$ is a constant coming from the integrations. The renormalization of the bare three-loop result, Eq. (B4), is performed in the next appendix by introducing appropriate counterterms.

APPENDIX C: RENORMALIZATION OF THE THREE-LOOP FREE ENERGY

Here, we give details on the renormalization procedure used. At order δ^2 new counterterms, which do not possess the form of the original tree-level Lagrangian, appear. This clearly is a manifestation, within our OPT framework, of perturbative nonrenormalizability. These counterterms originate from higher momentum-dependent divergences of some of the two-loop fermion self-energies shown in Fig. 1, and then potentially enter as contributions to the three-loop effective potential (or equivalently the free energy). Since the model is renormalizable in the $1/N$

expansion, it is clear that these nonrenormalizable counterterms are perturbative artifacts, which can be seen indeed to disappear in the corresponding $1/N$ quantities, as we will briefly show below. But since we are not using the $1/N$ expansion explicitly in our framework we have to deal to some extent with these nonrenormalizable terms. As we shall see below, however, the nonrenormalizable contributions to the effective potential actually vanish, such that only standard mass, wave function, and zero point energy counterterms are necessary to cancel the divergences (though this feature is simply an accident of the effective potential calculated at the second perturbative order).

At order δ^2 we have three two-loop contributions to the fermionic self-energy as shown in Fig. 1. From those, only the two displayed in Fig. 14 are divergent and will be evaluated here in detail. First, note that by choosing the momenta routing in an appropriate manner as indicated in Fig. 14 one only needs to evaluate the first graph since the closed fermionic loop contributes with $-4N$. One may explicitly verify that $\Sigma_b(p) + \Sigma_c(p) = [1 - 1/(4N)]\Sigma_b(p)$. With the LDE Feynman rules at $T = 0$ and $\mu = 0$ one has⁵

$$-i\Sigma_b(p) = -(-i\delta)^4 \left(\frac{-i\lambda}{\delta N}\right)^2 \int \frac{d^d k}{(2\pi)^d} \frac{d^d q}{(2\pi)^d} \frac{i(\not{k} + \eta)}{(q^2 - \eta^2)} \times \text{tr} \left\{ \frac{i(\not{k} + \eta)}{(k^2 - \eta^2)} \frac{i[(\not{k} + \not{p} - \not{q}) + \eta]}{[(k + p - q)^2 - \eta^2]} \right\}. \quad (\text{C1})$$

Here all integrals are done in arbitrary dimension $d = 3 - \epsilon$. Then, after taking the trace we have

$$\Sigma_b(p) = -\delta^2 \frac{4\lambda^2}{N} (i)^2 \int \frac{d^d k}{(2\pi)^d} \frac{d^d q}{(2\pi)^d} \frac{(\not{k} + \eta)}{(q^2 - \eta^2)} \times \frac{[k^2 + k(p - q) + \eta^2]}{(k^2 - \eta^2)[(k + p - q)^2 - \eta^2]}. \quad (\text{C2})$$

Now one can introduce one Feynman parameter (α) to merge the two k dependent propagators. Then, one performs a Wick rotation (using dimensional regularization in the $\overline{\text{MS}}$ scheme) to carry on the integral over k . This yields

$$\Sigma_b(p) = -\delta^2 \frac{4\lambda^2}{N(4\pi)^{3/2}} (e^{\gamma_E} M^2)^{\epsilon/2} \Gamma(\epsilon/2 - 1/2)(2 - \epsilon) \times \int_0^1 d\alpha [\alpha(1 - \alpha)]^{1/2 - \epsilon/2} \int \frac{d^d q_E}{(2\pi)^d} \times \frac{-\not{q}_E + \eta}{(q_E^2 + \eta^2)[(p - q)_E^2 + \eta_\alpha^2]^{-1/2 + \epsilon/2}}, \quad (\text{C3})$$

$$[\Sigma_b(p) + \Sigma_c(p)]_{\text{WFdiv}} = \frac{-\delta^2 \lambda^2}{(4\pi)^3} \frac{4}{N} \left(1 - \frac{1}{4N}\right) (e^{\gamma_E} M^2)^{\epsilon} \Gamma(\epsilon - 1)(2 - \epsilon) \int_0^1 d\alpha d\beta [\alpha(1 - \alpha)]^{(1/2) - (\epsilon/2)} (1 - \beta)^{-(1/2) + (\epsilon/2)} \times \frac{P}{(\eta_{\alpha,\beta}^2)^{\epsilon - 1}}, \quad (\text{C8})$$

where $\eta_\alpha^2 = \eta^2/[\alpha(1 - \alpha)]$. Now, one can use a second Feynman parameter (β) to merge the two final propagators, obtaining

$$\Sigma_b(p) = -\delta^2 \frac{4\lambda^2}{N(4\pi)^3} (e^{\gamma_E} M^2)^{\epsilon} \Gamma(\epsilon - 1)(2 - \epsilon) \times \int_0^1 d\alpha d\beta [\alpha(1 - \alpha)]^{1/2 - \epsilon/2} (1 - \beta)^{-3/2 + \epsilon/2} \times \frac{[\not{p}(1 - \beta) + \eta]}{(\eta_{\alpha,\beta}^2)^{\epsilon - 1}}, \quad (\text{C4})$$

where

$$\eta_{\alpha,\beta}^2 = -p^2(1 - \beta)\beta + \eta^2\beta + \eta_\alpha^2(1 - \beta). \quad (\text{C5})$$

Note that in the above equations we have already returned to Minkowski space. Let us now examine the type of divergences and corresponding counterterms emerging from these two-loop fermion self-energy expressions. The counterterms appear in the Lagrangian density $\mathcal{L}_{\text{ct}}^\delta$:

$$\mathcal{L}_{\text{ct}}^\delta = \bar{\psi}_k [i\not{A}^\delta(\eta)] \psi_k + B^\delta(\eta) \bar{\psi}_k \psi_k, \quad (\text{C6})$$

which is to be added to the original Lagrangian density, Eq. (3.1). The perturbative order at which the required counterterm contributions enter first can be readily found from Eq. (4.5):

$$\frac{V_{\text{eff,ct}}}{N}(\sigma_c, \eta) = i \int \frac{d^d p}{(2\pi)^d} \text{tr} \ln [\not{p}(1 + A^\delta) - \eta(1 + B^\delta)], \quad (\text{C7})$$

where, implicitly, those counterterm coefficients are of order $(\delta\lambda)^2$ (since at lowest $\lambda\delta$ order, all calculations are finite in dimensional regularization as we saw in Sec. III and IV). These counterterms are extracted from the \not{p} and η dependent terms in Eq. (C4). For the \not{p} term, for instance:

⁵The minus sign due to the fermionic loop has already been taken into account in Eq. (C1).

where the only pole is contained in $\Gamma(\epsilon - 1)$. One can then expand in ϵ and perform the (finite) integrals in α and β to obtain a counterterm as $\not{p}A^\delta(\eta, p)$, where

$$A^\delta(\eta, p) = -\delta^2 \frac{\lambda^2}{(4\pi)^3} \frac{4}{N} \left(1 - \frac{1}{4N}\right) \frac{\pi}{15\epsilon} (-p^2 + 25\eta^2). \quad (\text{C9})$$

Similarly the other counterterm can be extracted from the η dependent term in Eq. (C4):

$$[\Sigma_b(p) + \Sigma_c(p)]_{\text{massdiv}} = \frac{-\delta^2 \lambda^2}{(4\pi)^3} \frac{4}{N} \left(1 - \frac{1}{4N}\right) (e^{\gamma_E} M^2)^\epsilon \Gamma[\epsilon - 1] (2 - \epsilon) \int_0^1 d\alpha d\beta [\alpha(1 - \alpha)]^{(1/2) - (\epsilon/2)} (1 - \beta)^{-(3/2) + (\epsilon/2)} \times \frac{\eta}{(\eta_{\alpha,\beta}^2)^{\epsilon-1}}. \quad (\text{C10})$$

The same types of manipulations that lead to the pole in Eq. (C9) above fix the other counterterm as $\eta B^\delta(\eta, p)$, where

$$B^\delta(\eta, p) = \delta^2 \frac{\lambda^2}{(4\pi)^3} \frac{4}{N} \left(1 - \frac{1}{4N}\right) \frac{\pi}{3\epsilon} (-p^2 + 9\eta^2). \quad (\text{C11})$$

Note in Eqs. (C9) and (C11) the extra p^2 dependence which is the manifestation of the perturbative nonrenormalizability.

As mentioned above, all such nonrenormalizable terms should be absent in the renormalizable $1/N$ expansion. More precisely, one can check this at the next-to-leading $1/N$ order where the equivalent contribution to the fermion self-energy is shown in Fig. 15 (which corresponds to an infinite sum of perturbative one-loop graphs). We can easily obtain the structure of the divergent terms, replacing expression (C9) and (C11) in dimensional regularization as

$$\frac{1}{N\pi^2} \frac{1}{\epsilon} \left(\frac{\not{p}}{3} + \eta\right), \quad (\text{C12})$$

where we used expression (2.12b) of Ref. [24] for the $d = 2 + 1$ resummed σ -propagator. The expression (C12) is consistent with the calculation of the wave function and mass counterterm as performed in Ref. [24] with cutoff regularization. The crucial point in the $1/N$ expansion is that the resummed σ propagator has the nonperturbative $|p|^{-1}$ behavior [24] at large $|p|$, thus damping the degree of divergences with respect to usual perturbative graphs (such as those in Fig. 14) and thus the absence of momentum-dependent divergences in Eq. (C12). Nevertheless, since our construction relies on standard perturbation, in princi-

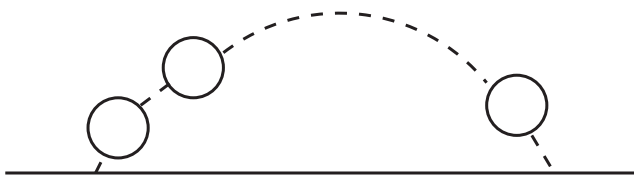


FIG. 15. Next-to-leading order in the $1/N$ expansion graphs contributing to the fermionic self-energy.

ple we would have to introduce corresponding new counterterms, with higher derivatives, into the Lagrangian at this perturbative order. But actually these p -dependent pieces' contributions are canceled in the free energy graphs, as we will see next, so that it is not needed to deal with these extra nonrenormalizable terms. Inserting the above two-loop counterterms into the (one-loop) free energy graph, for instance for the A counterterm in Eq. (C9), yields

$$\frac{V_{\text{eff}}^A}{N} = -i \int \frac{d^d p}{(2\pi)^d} \text{tr} \frac{\not{p} - \eta}{p^2 - \eta^2} A^\delta(\eta), \quad (\text{C13})$$

which gives, after taking the trace and going to Euclidean momenta,

$$\frac{V_{\text{eff}}^A}{N} = \delta^2 \frac{8\lambda^2 \eta^2}{5\epsilon(4\pi)^2} \frac{4}{N} \left(1 - \frac{1}{4N}\right) \int \frac{d^d p_E}{(2\pi)^d} \frac{p_E^2}{p_E^2 + \eta^2}, \quad (\text{C14})$$

where we simply used for the integrand $p^2/(p^2 + \eta^2) = 1 - \eta^2/(p^2 + \eta^2)$. Note also that the integral $\int d^n p p^2$ is zero in dimensional regularization, so that only a mass-dependent divergence remained in Eq. (C14) and we finally obtain

$$\frac{V_{\text{eff}}^A}{N} = \delta^2 \eta^5 \frac{8\lambda^2}{5(4\pi)^3} \frac{4}{N} \left(1 - \frac{1}{4N}\right) \left[\frac{1}{\epsilon} - \ln\left(\frac{\eta}{M}\right) + 1 - \ln 2 \right]. \quad (\text{C15})$$

Similarly, for

$$\frac{V_{\text{eff}}^B}{N} = i \int \frac{d^d p}{(2\pi)^d} \text{tr} \frac{\not{p} - \eta}{p^2 - \eta^2} B^\delta(\eta), \quad (\text{C16})$$

one obtains⁶

⁶Note that the final mass and wave function counterterms are proportional to $\lambda^2 \eta^2$, which simply reflects that the coupling λ of the 3 dimensional GN model has mass dimension -1 , i.e., the counterterms coefficients are actually dimensionless.

$$\frac{V_{\text{eff}}^B}{N} = -\delta^2 \eta^5 \frac{8\lambda^2}{3(4\pi)^3} \frac{4}{N} \left(1 - \frac{1}{4N}\right) \left[\frac{1}{\epsilon} - \ln\left(\frac{\eta}{M}\right) + 1 - \ln 2 \right]. \quad (\text{C17})$$

Next, the contributions in Eqs. (C15) and (C17) should be added in the $\overline{\text{MS}}$ scheme to the bare three-loop free energy expression (B4). This leaves a remaining divergent contribution:

$$\frac{V_{\text{eff}}^{c+d+A+B}}{N} = \delta^2 \eta^5 \frac{\lambda^2}{15(4\pi^3)} \frac{4}{N} \left(1 - \frac{1}{4N}\right) \frac{1}{\epsilon}, \quad (\text{C18})$$

which is finally renormalized by an additional vacuum (free energy) counterterm. This additional counterterm is

expected, since the free energy is a composite operator, and is needed similarly in the (renormalizable) $d = 1 + 1$ GN model, as shown in a previous reference [13]. Note that, although the perturbative nonrenormalizability manifests itself at order δ^2 by the presence of the higher derivative divergences in Eqs. (C9) and (C11), corresponding counterterms are not needed for the quantities (and perturbative order) we restrict ourselves to. Thus the arbitrariness in the final renormalized free energy is not more than the usual renormalization scale introduced from dimensional regularization. The complete renormalized three-loop contribution to the free energy is obtained, in the $\overline{\text{MS}}$ scheme, by adding all the finite contributions as given in Eqs. (6.6), (6.7), (C15), and (C17), respectively, leads to the final expression, Eq. (6.8).

-
- [1] D. Gross and A. Neveu, Phys. Rev. D **10**, 3235 (1974).
[2] O. Schnetz, M. Thies, and K. Urlichs, Ann. Phys. (N.Y.) **314**, 425 (2004); M. Thies, J. Phys. A **39**, 12707 (2006).
[3] A. Chodos and H. Minakata, Nucl. Phys. **B490**, 687 (1997).
[4] K. G. Klimenko, Z. Phys. C **37**, 457 (1988); B. Rosenstein, S. H. Park, and B. J. Warr, Phys. Rev. D **39**, 3088 (1989); Phys. Rev. Lett. **62**, 1433 (1989).
[5] S. Coleman, *Aspects of Symmetry* (Cambridge University Press, Cambridge, England, 1985).
[6] M. Moshe and J. Zinn-Justin, Phys. Rep. **385**, 69 (2003).
[7] U. Wolff, Phys. Lett. **157B**, 303 (1985).
[8] A. Barducci, R. Casalbuoni, M. Modugno, and G. Pettini, Phys. Rev. D **51**, 3042 (1995).
[9] N. D. Mermin and H. Wagner, Phys. Rev. Lett. **17**, 1133 (1966); S. Coleman, Commun. Math. Phys. **31**, 259 (1973); L. D. Landau and E. M. Lifshitz, *Statistical Physics* (Pergamon, New York, 1958), p. 482.
[10] R. F. Dashen, S.-K. Ma, and R. Rajaraman, Phys. Rev. D **11**, 1499 (1975).
[11] J. B. Kogut and C. G. Strouthos, Phys. Rev. D **63**, 054502 (2001).
[12] S. Hands, K. Kocic, and J. B. Kogut, Ann. Phys. (N.Y.) **224**, 29 (1993); Nucl. Phys. **B390**, 355 (1993).
[13] J.-L. Kneur, M. B. Pinto, and R. O. Ramos, Phys. Rev. D **74**, 125020 (2006); Braz. J. Phys. **37**, 258 (2007).
[14] S. K. Gandhi, H. F. Jones, and M. B. Pinto, Nucl. Phys. **B359**, 429 (1991).
[15] J.-L. Kneur, M. B. Pinto, and R. O. Ramos, Phys. Rev. Lett. **89**, 210403 (2002); Phys. Rev. A **68**, 043615 (2003).
[16] E. Braaten and E. Radescu, Phys. Rev. Lett. **89**, 271602 (2002); Phys. Rev. A **66**, 063601 (2002).
[17] J.-L. Kneur, A. Neveu, and M. B. Pinto, Phys. Rev. A **69**, 053624 (2004); J.-L. Kneur and M. B. Pinto, Phys. Rev. A **71**, 033613 (2005); B. Kastening, Phys. Rev. A **70**, 043621 (2004).
[18] J.-L. Kneur, M. B. Pinto, R. O. Ramos, and E. Staudt, arXiv:0705.0673.
[19] J. I. Kapusta, *Finite-Temperature Field Theory* (Cambridge University Press, Cambridge, England, 1985); M. Le Bellac, *Thermal Field Theory* (Cambridge University Press, Cambridge, England, 1996).
[20] A. Okopinska, Phys. Rev. D **35**, 1835 (1987); M. Moshe and A. Duncan, Phys. Lett. B **215**, 352 (1988).
[21] R. Seznec and J. Zinn-Justin, J. Math. Phys. (N.Y.) **20**, 1398 (1979); J. C. Le Guillou and J. Zinn-Justin, Ann. Phys. (N.Y.) **147**, 57 (1983); V. I. Yukalov, Moscow University Physics Bulletin **31**, 10 (1976); W. E. Caswell, Ann. Phys. (N.Y.) **123**, 153 (1979); I. G. Halliday and P. Suranyi, Phys. Lett. **85B**, 421 (1979); J. Killinbeck, J. Phys. A **14**, 1005 (1981); R. P. Feynman and H. Kleinert, Phys. Rev. A **34**, 5080 (1986); H. F. Jones and M. Moshe, Phys. Lett. B **234**, 492 (1990); A. Neveu, Nucl. Phys. B, Proc. Suppl. **18**, 242 (1991); V. Yukalov, J. Math. Phys. (N.Y.) **32**, 1235 (1991); C. M. Bender *et al.*, Phys. Rev. D **45**, 1248 (1992); S. Gandhi and M. B. Pinto, Phys. Rev. D **46**, 2570 (1992); H. Yamada, Z. Phys. C **59**, 67 (1993); A. N. Sissakian, I. L. Solovtsov, and O. P. Solovtsova, Phys. Lett. B **321**, 381 (1994); H. Kleinert, Phys. Rev. D **57**, 2264 (1998); Phys. Lett. B **434**, 74 (1998); for a review, see H. Kleinert and V. Schulte-Frohlinde, *Critical Properties of ϕ^4 -Theories* (World Scientific, Singapore, 2001), Chap. 19; K. G. Klimenko, Z. Phys. C **50**, 477 (1991); **60**, 677 (1993); Mod. Phys. Lett. A **9**, 1767 (1994); M. B. Pinto, R. O. Ramos, and P. J. Sena, Physica A (Amsterdam) **342**, 570 (2004).
[22] M. B. Pinto and R. O. Ramos, Phys. Rev. D **60**, 105005 (1999); **61**, 125016 (2000).
[23] C. Arvanitis, F. Geniet, M. Iacomi, J.-L. Kneur, and A. Neveu, Int. J. Mod. Phys. A **12**, 3307 (1997).
[24] B. Rosenstein, B. Warr, and S. H. Park, Phys. Rep. **205**, 59 (1991).
[25] J. C. Collins, *Renormalization* (Cambridge University

Press, Cambridge, England, 1984).

- [26] J. Bijnens, Prog. Part. Nucl. Phys. **58**, 521 (2007).
- [27] P.M. Stevenson, Phys. Rev. D **23**, 2916 (1981); Nucl. Phys. **B203**, 472 (1982).
- [28] R. Root, Phys. Rev. D **11**, 831 (1975).
- [29] P. Castorina, M. Mazza, and D. Zappala, Phys. Lett. B **567**, 31 (2003).
- [30] *Handbook of Mathematical Functions*, edited by M. Abramowitz and I.A. Stegun (Dover, New York, 1972), 9th ed..
- [31] MATHEMATICA version 5.2, Wolfram Research.